ORIGINAL PAPER

A defined clathrin-mediated trafficking pathway regulates sFLT1/VEGFR1 secretion from endothelial cells

Karina Kinghorn[1] · Amy Gill[6] · Allison Marvin[2] · Renee Li[2] · Kaitlyn Quigley[2] · Simcha Singh[2] ·
Michaelanthony T. Gore[2] · Ferdinand le Noble[5] · Feilim Mac Gabhann[6] · Victoria L. Bautch[1,2,3,4]

Abstract

FLT1/VEGFR1 negatively regulates VEGF-A signaling and is required for proper vessel morphogenesis during vascular development and vessel homeostasis. Although a soluble isoform, sFLT1, is often mis-regulated in disease and aging, how sFLT1 is trafficked and secreted from endothelial cells is not well understood. Here we define requirements for constitutive sFLT1 trafficking and secretion in endothelial cells from the Golgi to the plasma membrane, and we show that sFLT1 secretion requires clathrin at or near the Golgi. Perturbations that affect sFLT1 trafficking blunted endothelial cell secretion and promoted intracellular mis-localization in cells and zebrafish embryos. siRNA-mediated depletion of specific trafficking components revealed requirements for RAB27A, VAMP3, and STX3 for post-Golgi vesicle trafficking and sFLT1 secretion, while STX6, ARF1, and AP1 were required at the Golgi. Live-imaging of temporally controlled sFLT1 release from the endoplasmic reticulum showed clathrin-dependent sFLT1 trafficking at the Golgi into secretory vesicles that then trafficked to the plasma membrane. Depletion of STX6 altered vessel sprouting in 3D, suggesting that endothelial cell sFLT1 secretion influences proper vessel sprouting. Thus, specific trafficking components provide a secretory path from the Golgi to the plasma membrane for sFLT1 in endothelial cells that utilizes a specialized clathrin-dependent intermediate, suggesting novel therapeutic targets.

Keywords sFLT1 · Secretion · Golgi · AP1 · Clathrin · vWF

Introduction

Blood vessels form early during vertebrate embryonic development to deliver oxygen and nutrients to developing tissues and organs, and in adults blood vessels also regulate organ function and homeostasis [1–3]. Endothelial progenitor cells initially coalesce to create vessels that differentiate through a process called vasculogenesis, and new vessels then arise from existing vessels primarily via sprouting angiogenesis to expand the vascular network [4–6]. Numerous signaling pathways regulate angiogenic sprouting and crosstalk with each other, and signaling amplitude is often controlled by endothelial cell-intrinsic negative regulators of the pathways. Thus, endothelial cells are crucial players in angiogenic pathway regulation during blood vessel formation and function.

Among the signals important to sprouting angiogenesis, vascular endothelial growth factor-A (VEGF-A)-mediated signaling stands out, as it is required in almost all tissues for proper blood vessel formation [7–9]. The VEGF-A ligand

✉ Victoria L. Bautch
bautch@med.unc.edu

1   Curriculum in Cell Biology and Physiology, University of North Carolina, Chapel Hill, NC, USA

2   Department of Biology, The University of North Carolina at Chapel Hill, CB No. 3280, Chapel Hill, NC 27599, USA

3   McAllister Heart Institute, University of North Carolina, Chapel Hill, NC, USA

4   UNC Lineberger Comprehensive Cancer Center, University of North Carolina, Chapel Hill, NC, USA

5   Department of Cell and Developmental Biology, Institute of Zoology, Karlsruhe Institute of Technology, Karlsruhe, Germany

6   Department of Biomedical Engineering, Institute for Computational Medicine, Johns Hopkins University, Baltimore, MD, USA

is alternatively spliced to produce several isoforms that differentially interact with the extracellular matrix (ECM) and thus provide spatial cues and survival signals to endothelial cells in emerging vessels [10]. Endothelial cells often respond to VEGF-A signals by adopting a migratory tip cell phenotype or a more proliferative stalk cell phenotype to extend the sprout [11, 12]. Among endothelial cell VEGF-A receptors, VEGFR2 (FLK1) and VEGFR1 (FLT1) provide the primary pro- and anti-angiogenic signals, respectively. Tip cells express higher levels of VEGFR2 that promote migration, while stalk cells express higher levels of FLT1 [4, 13]. FLT1 is alternatively spliced to produce a full-length transmembrane isoform (mFLT1) and a secreted soluble isoform (sFLT1) [14, 15]. Both FLT1 isoforms bind VEGF with a 10-fold higher affinity than VEGFR2 and can act as decoys to sequester excess VEGF-A ligand [16, 17]. FLT1, VEGFR2, and VEGF-A are all required for blood vessel formation, as genetic loss leads to severe vascular defects and early embryonic lethality in mice [18–21]. However, FLT1 signaling via its cytoplasmic tyrosine kinase domain is not required for vascular development or viability, as mice lacking the cytoplasmic portion of FLT1 survive without defects in vascular development, and mice expressing only sFLT1 have significant viability [22, 23]. sFLT1 secretion is upregulated in response to hypoxia and is associated with endothelial cell dysfunction during aging, chronic kidney disease, and COVID-19 infection [24–27]. Thus, negative regulation of VEGF-A signaling through FLT1 is required for proper vascular development, and dysregulation is associated with vascular pathology and aging.

sFLT1 is secreted from endothelial cells and binds the ECM via poorly-defined heparin-binding sites, thus acting as a critical molecular rheostat to modulate ligand availability extracellularly [28]. sFLT1 is also expressed by non-endothelial cells including trophoblasts, macrophages, and specialized pericytes such as podocytes, but its secretion is not well-defined in these cells [29–35]. Endothelial sFLT1 is a predominant regulator of developmental angiogenic sprouting. In mouse embryonic stem cell-derived *Flt1*$^{-/-}$ mutant vessels, genetic rescue with either endothelial cell-expressed *mFlt1* or *sFlt1* restored proper VEGFR2 signaling and endothelial cell proliferation, but only *sFlt1* effectively rescued branching morphogenesis [36]. Additionally, *sFlt1* expression from the lateral base area of new sprouts restored the ability of emerging sprouts to extend away from the parent vessel that was lost with *Flt1* deletion [37, 38]. These findings support a local sprout guidance model, positing that stalk cell secretion of sFLT1 neutralizes VEGF-A next to the sprout base, thus establishing a forward guide for tip cells as they migrate away from the parent vessel. In zebrafish, genetic loss of both *mflt1* and *sflt1* leads to ectopic sprouting of intersegmental vessels, while expression of only *sflt1* was

sufficient for proper vessel formation [39, 40]. Together, these data suggest that secreted sFLT1 interactions in the ECM are critical for regulating blood vessel development and patterning. Despite this required function for sFLT1, the mechanisms regulating sFLT1 trafficking and secretion from endothelial cells remain largely unknown.

Secreted proteins traffic through the endoplasmic reticulum (ER) to the Golgi, where they load into vesicles for transport to the plasma membrane and secretion [41]. Major secretion routes include constitutive vesicle transport from the Golgi to the plasma membrane, intermediate sorting to specialized vesicles, or stimulus-regulated fusion and release from large storage granules [42]. ARF (ADP-ribosylation factor) GTPases, RAB GTPases, SNAREs (Soluble NSF Attachment Protein Receptors), and coat proteins regulate the sorting and trafficking of proteins into these different pathways [43–49]. Movement from the Golgi to the plasma membrane is facilitated in some cases via a "sorting center" that utilizes proteins like AP1 and STX6 to move proteins into the different pathways [50–55]. However, it is largely not known how specific trafficking components interact in sFLT1 trafficking and secretion.

von Willebrand Factor (vWF) release from Weibel-Palade bodies upon histamine stimulation is a well-characterized secretory pathway in endothelial cells [56]. These large storage granules are held at the plasma membrane until stimulus-promoted release of contents [57–60], and vWF is also constitutively secreted through Golgi-derived vesicles or via spontaneous release of Weibel-Palade bodies [61, 62] using poorly defined pathways. Although numerous other proteins are associated with Weibel-Palade bodies, sFLT1 has not been detected in Weibel-Palade bodies [63], and the trafficking/secretion pathway for sFLT1 has not been well-defined. sFLT1 secretion is constitutive, as it is found in human plasma and endothelial cell conditioned media absent stimulation [30, 64, 65], and secretion is further stimulated by hypoxia [66–68]. Stable overexpression of sFLT1 revealed a requirement for several ARFs and RAB11 in trafficking the labeled protein [69], but no studies have systematically defined how sFLT1 is trafficked through endothelial cells to the plasma membrane for secretion.

Here, we define a trafficking/secretion pathway for sFLT1 in endothelial cells that requires intermediate sorting via clathrin prior to constitutive secretion. Surprisingly, sFLT1 secretion utilizes trafficking components that are typically associated with secretory granule maturation such as AP1-dependent clathrin assembly and STX6 at the Golgi. Perturbations that affect secretion also mis-localize sFLT1 in endothelial cells in vitro and in vivo and affect 3D vascular sprouting. Thus, endothelial cell sFLT1 is trafficked by several regulators prior to its secretion, and this novel pathway provides new therapeutic targets for treatment of endothelial cell dysfunction.

Results

sFLT1 is constitutively secreted from endothelial cells

Although it is well-established that soluble FLT1 (sFLT1) is secreted from endothelial cells [14, 69], the pathway utilized by sFLT1 for trafficking and secretion is poorly described. To define a pathway from synthesis to secretion in endothelial cells, we first confirmed that sFLT1 is robustly secreted from primary human umbilical vein endothelial cells (HUVEC) absent stimulation. Concentrated conditioned media and lysates of HUVEC but not normal human lung fibroblast (NHLF) controls contained a 90 kDa protein that reacted with a FLT1 antibody and was the expected size for sFLT1 (Fig. 1A). The antibody was validated with selective manipulation of the two
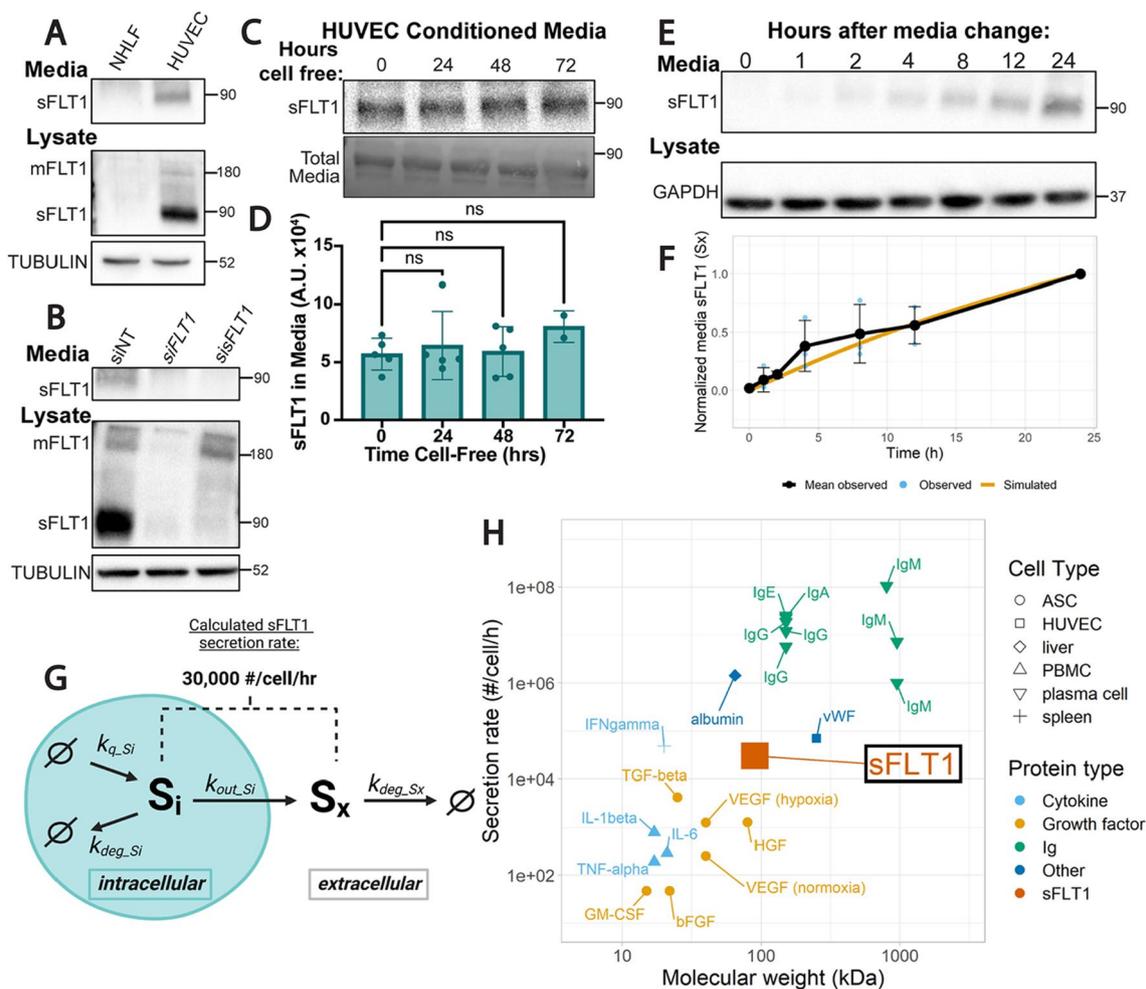

Fig. 1 sFLT1 is constitutively secreted from endothelial cells. **A** Immunoblot of FLT1 in concentrated conditioned media or cell lysates of normal human lung fibroblasts (NHLF) or human umbilical vein endothelial cells (HUVEC). Tubulin loading control. Representative of 3 replicates. **B** Immunoblot of FLT1 in concentrated conditioned media or lysates of HUVEC transfected with siRNAs targeting mFLT1 and sFLT1 (si*FLT1*), sFLT1 (si*sFLT1*), or non-targeting control (siNT). Tubulin loading control. Representative of 3 replicates. **C** Top: representative immunoblot of sFLT1 in concentrated conditioned media from HUVEC incubated cell-free for indicated times. Bottom: total media protein loading control. **D** Quantification of FLT1 band intensity from 1 C. Shown are means +/− SD of n = 2–5 replicates/condition. **E** Representative immunoblot of sFLT1 in HUVEC concentrated conditioned media for the indicated time points following media change. GAPDH loading control. **F** Graph of sFLT1 media/time. Black line: densitometric analysis of sFLT1 from 1E, with media sFLT1 normalized to intensity at 24 h (n = 3 replicates). Blue dots and error bars: Means +/− SD of n = 3 replicates/condition. Orange line: simulation of secreted sFLT1 from literature-based computational model [69, 123]. **G** Diagram of processes included in the mechanistic computational model of sFLT1 secretion, with the calculated secretion rate noted. Schematic created with BioRender.com. **H** Comparison of sFLT1 secretion rate predicted by computational model vs. molecular weight to that of other secreted proteins (See Suppl. Table S5). *ASC* adipose stromal cell, *HUVEC* human umbilical vein endothelial cell, *Ig* immunoglobulin, *PBMC* peripheral blood mononuclear cell

FLT1 isoforms, mFLT1 and sFLT1, via siRNA depletion. siRNA targeting both FLT1 isoforms (si*FLT1*) reduced both expected 180 kDa mFLT1 and 90 kDa sFLT1 bands, while siRNA selectively targeting sFLT1 (si*sFLT1*) [70] reduced the 90 kDa sFLT1 band in media and lysates but not the 180 kDa mFLT1 band in lysates (Fig. 1B). Thus, sFLT1 is constitutively secreted by endothelial cells and accumulates to detectable intracellular levels in HUVEC.

To determine the basal rate of sFLT1 secretion from endothelial cells, we analyzed sFLT1 protein levels in media and lysate collected from HUVEC over time. We first assessed extracellular sFLT1 stability and saw no significant decrease in levels in media removed from cells for further incubation up to 72 h (Fig. 1C, D), allowing us to equate media protein levels with secreted protein levels over time (Fig. 1E). We next temporally quantified sFLT1 levels after a media change and compared these data to predictions from a newly generated mechanistic computational model of sFLT1 secretion (Fig. 1F, G; Methods; Suppl. Fig. 1A). For the computational model, rate parameters were derived from published time course data of sFLT1 secretion (Suppl. Tables S1–S4). The model parameters are well-constrained by the previous data, with low uncertainty in the optimal values (Suppl. Fig. 1B–D), and they also simulate the data in this study well (Fig. 1F). As a result, we estimate that sFLT1 is constitutively secreted at a constant rate of approximately 30,000 molecules/cell/hr (Fig. 1G). This value is comparable to the constitutive secretion rate of vWF in HUVEC [71], faster than the published secretion rate of VEGF-A and other cytokines/growth factors from adipose stromal cells and peripheral blood mononuclear cells [72, 73], and slower than published rates of immunoglobulin secretion from plasma cells or albumin from liver cells [74–79] (Fig. 1H, Suppl. Table S5). These data are consistent with sFLT1 being produced and secreted at physiologically relevant levels by HUVEC, and confidence in the secretion estimate is enhanced by consistency across multiple independent experiments by different groups. The model also gives insight into relationships between mechanistic processes affecting sFLT1; for example, the modeling suggests that an intracellular sFLT1 molecule has a roughly equal probability of being secreted or intracellularly degraded (Suppl. Table S4).

Intracellular sFLT1 is Golgi-localized prior to secretion

To begin defining how sFLT1 is trafficked in endothelial cells, we determined sFLT1 subcellular localization. C-terminal HA-tagged human sFLT1 (sFLT1-HA) was introduced to non-endothelial cells, and immunoblot analysis confirmed that both cell-associated and secreted sFLT1-HA were detected by HA and FLT1 antibodies (Suppl. Fig. 2A).

sFLT1-HA was also detected in conditioned media and lysate from transfected HUVEC with both HA and FLT1 antibodies (Fig. 2A). Immunofluorescence imaging of sFLT1-HA intracellular localization showed that sFLT1-HA colocalized with the trans-Golgi marker (γ-Adaptin) in both non-endothelial cells and HUVEC, consistent with previous reports of Golgi localization [69, 80] (Fig. 2B, B′, Suppl. Fig. 2B, B′). Staining for endogenous FLT1 revealed a similar Golgi localization in HUVEC that colocalized with γ-Adaptin (Fig. 2C, C′). The FLT1 antibody reactivity was specific to HUVEC and not NHLF controls, and FLT1 signal was depleted following si*FLT1* and si*sFLT1* treatments compared to controls (Suppl. Fig. 2C, D). We next examined sFLT1 localization by subcellular fractionation via density gradient ultracentrifugation of HUVEC lysates, and confirmed that most sFLT1 protein is found in fractions that also express the trans-Golgi marker, STX6, with lesser amounts seen in fractions that express the ER marker calnexin, and in vesicle/plasma membrane fractions (Fig. 2D). Therefore, prior to secretion from endothelial cells, sFLT1 is Golgi-localized, and minor depots of sFLT1 protein suggest it moves from the ER to the Golgi, and from the Golgi to cytoplasmic vesicles prior to secretion.

sFLT1 secretion from endothelial cells requires the Golgi, clathrin, and SNAREs

To establish broad requirements for sFLT1 trafficking and secretion in endothelial cells, primary endothelial cells were exposed to pharmacological inhibitors that block trafficking at specific steps of the trafficking process. Brefeldin-A blocks protein transport from the ER to the Golgi, and treatment led to significant reduction of sFLT1 in HUVEC conditioned media, while lysate levels trended towards a slight elevation (Fig. 3A, Suppl. Fig. 3A,G), consistent with constitutive trafficking of sFLT1 through the Golgi and confirming a previous report [69].

Although known for their involvement in endocytic recycling pathways [81], clathrin and dynamin also facilitate Golgi-to-vesicle trafficking [82–85]. Dynamin is implicated in constitutive secretion [86], while clathrin regulates specialized pathways such as Weibel-Palade body maturation that leads to vWF secretion [55]. To determine if sFLT1 constitutive trafficking and secretion are clathrin- or dynamin-dependent, HUVEC were treated with chlorpromazine to block clathrin-mediated or dynasore to block dynamin-mediated trafficking. Chlorpromazine treatment significantly reduced sFLT1 levels in the conditioned media, while lysate levels trended to increase (Fig. 3B, Suppl. Fig. 3B, H), indicating a role for clathrin-coated vesicles in sFLT1 secretion. sFLT1 levels in the media and lysates were unaltered
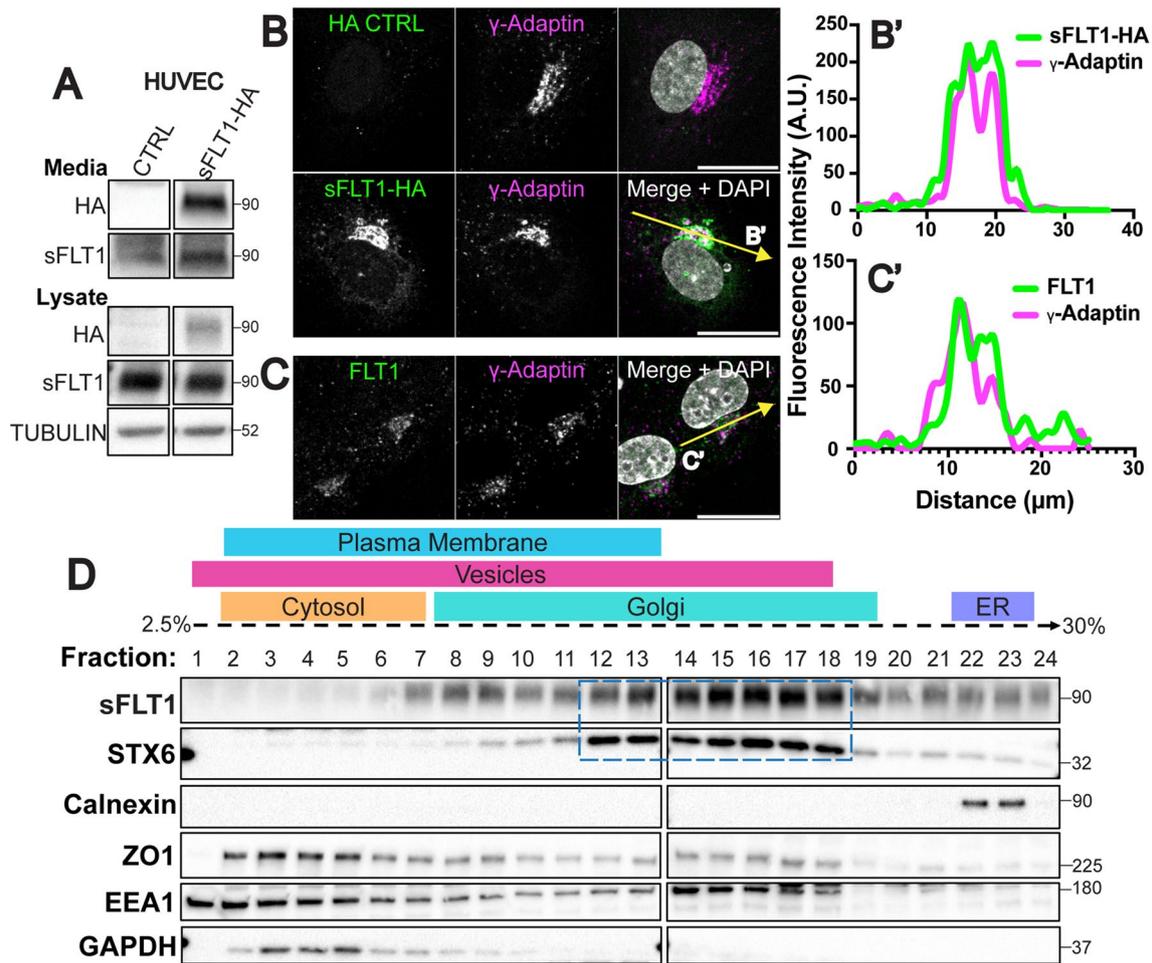
Fig. 2 Intracellular sFLT1 localizes to the Golgi in endothelial cells. **A** Immunoblot of sFLT1-HA in concentrated conditioned media or cell lysates of HUVEC transfected with indicated DNA and probed with indicated antibodies. Tubulin loading control. **B** HUVEC immunofluorescence of sFLT1-HA or control and stained for HA, γ-Adaptin (Trans-Golgi), and DAPI (nucleus). Scale bar, 20 μm. Yellow line, line scan. **B′** Line scan of sFLT1-HA and γ-Adaptin fluorescence intensity. **C** HUVEC immunofluorescence with indicated antibodies: FLT1, γ-Adaptin (Trans-Golgi), and DAPI (nucleus). Scale bar, 20 μm. Yellow line, line scan. **C′** Line scan of FLT1 and γ-Adaptin fluorescence intensity. **D** HUVEC density ultracentrifugation subcellular fractionation (see Methods for details). Dashed box, fractions positive for both sFLT1 and STX6 (trans-Golgi marker). Other markers: Calnexin (endoplasmic reticulum); ZO1 (plasma membrane); EEA1 (vesicles) GAPDH (cytosol). **A–D** n = 3 replicates

by dynasore; therefore, dynamins are likely not required for sFLT1 secretion (Fig. 3C, Suppl. Fig. 3C, I).

Next, we inhibited trafficking components that promote the release of secreted proteins from the plasma membrane. SNARE complexes fuse vesicles and target membranes; therefore, we inhibited SNARE disassembly with the NSF analog peptide, TATNSF700 [87] and found that sFLT1 secretion was reduced while cellular sFLT1 levels were minimally affected (Fig. 3D, Suppl. Fig. 3D, J). Cholesterol-enriched lipid rafts are sites of localized membrane trafficking [88, 89], and lipid rafts have been implicated in sFLT1 binding to the surface of podocytes [31]. We assessed the role of lipid rafts in sFLT1 secretion via cholesterol depletion using β-methyl--cyclodextrin; however, neither secreted or cell-associated endothelial sFLT1 levels were altered by cholesterol depletion (Fig. 3E, Suppl. Fig. 3E, K). Finally, endothelial sFLT1 degradation was interrogated with chloroquine treatment to block lysosome-mediated degradation. Both secreted and cell-associated sFLT1 accumulated following chloroquine treatment of endothelial cells, consistent with a lysosomal degradation mechanism for sFLT1 (Fig. 3F, Suppl. Fig. 3F, L). Computational analysis of secretion rate (k_{out_Si}) inhibition required to reproduce the experimentally observed sFLT1 changes suggested that brefeldin-A inhibits sFLT1 k_{out_Si} by 90% while both chlorpromazine and TATNSF700 inhibit by 60% (Fig. 3G; Suppl. Table S6), consistent with an absolute requirement for Golgi trafficking of sFLT1 and partial block of sFLT1 secretion by clathrin and
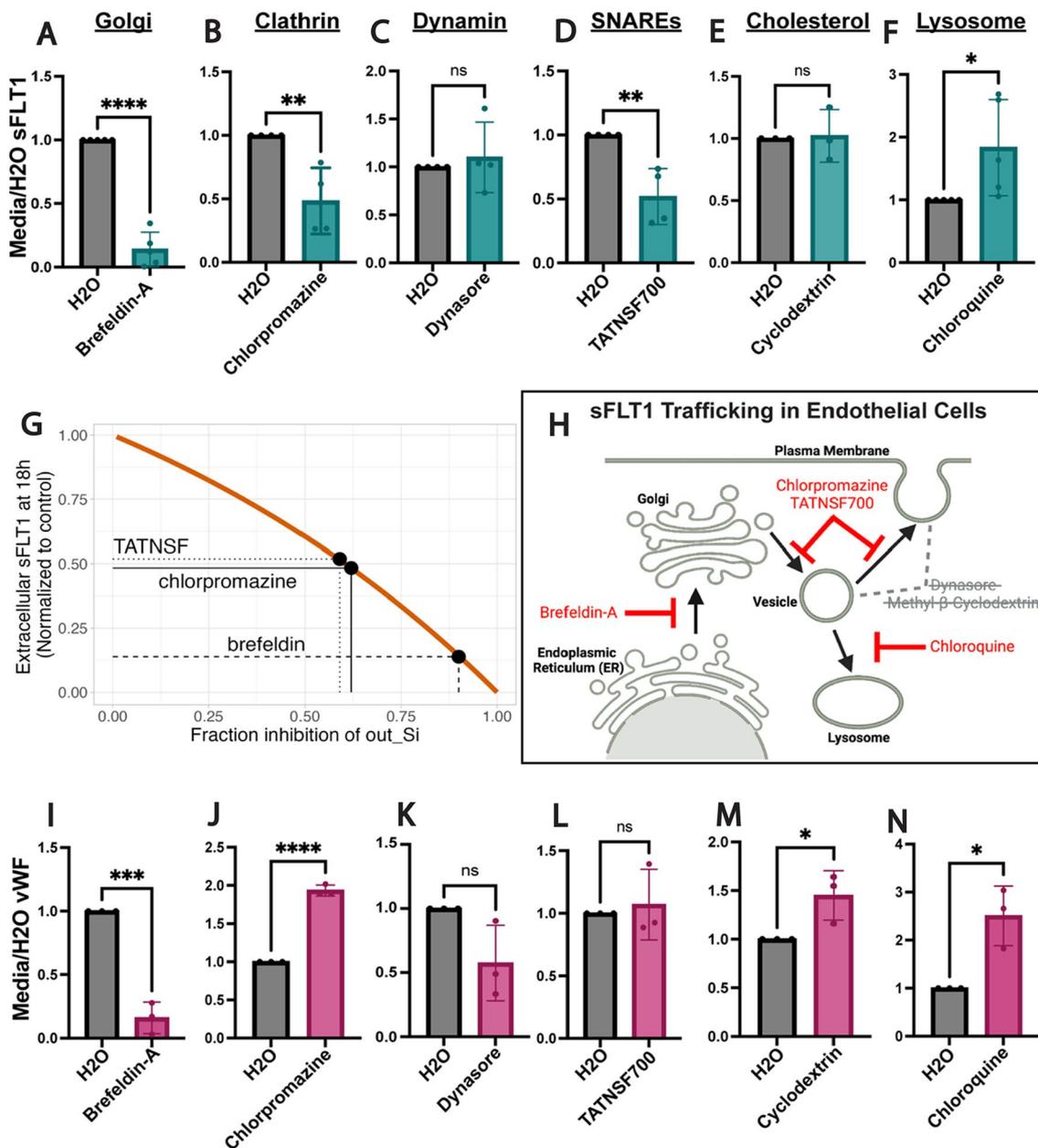
Fig. 3 Endothelial sFLT1 trafficking requires the Golgi, clathrin, and SNAREs. **A–F**, **I–N** Quantification of immunoblots of HUVEC treated as indicated (X-axis) prior to collection of concentrated media and incubated with FLT1 (**A–F**) or vWF (**I–N**) antibody and normalized to vehicle control. Mean +/− SD of experimental replicates shown. Statistics: student's two-tailed t-test, *P < 0.05, **P < 0.01, ***P < 0.001, ****P < 0.0001, ns, not significant. **G** Orange line: simulation of extracellular sFLT1 in 18 h media related to fraction inhibition of sFLT1 k_{out_Si}. Black dots: predicted fraction inhibition of k_{out_Si} by pharmacological inhibitor treatments. **H** Diagram of sFLT1 protein trafficking steps tested. Red: inhibitors that impacted sFLT1 secretion. Grey with cross-out: inhibitors that did not impact sFLT1 secretion. Created with Biorender.com

SNARE inhibition. In summary, pharmacological trafficking perturbations and computational analysis showed that endothelial sFLT1 constitutive secretion is dependent on ER to Golgi transport, that vesicle trafficking of sFLT1 from the Golgi to the plasma membrane is SNARE-dependent and unexpectedly dependent on clathrin, and that intracellular sFLT1 is degraded by the lysosome (Fig. 3H).

The requirements for endothelial sFLT1 secretion were then compared to requirements for constitutive secretion of vWF, an endothelial cell protein that is secreted both constitutively and upon stimulation via Weibel-Palade bodies [61, 62, 90, 91]. Constitutive vWF secretion was reduced by brefeldin-A treatment, which blocks ER to Golgi transport, and blockade of lysosomal degradation

via chloroquine increased vWF secretion, consistent with previous findings [61, 62] and similar to sFLT1 sensitivities (Fig. 3I, N; Suppl. Fig. 3G, L). However, several other manipulations produced different results between constitutive sFLT1 and vWF secretion profiles in endothelial cells. Secreted vWF significantly increased with clathrin blockade via chlorpromazine compared to reduced secretion of sFLT1 (Fig. 3J, Suppl. Fig. 3H). This increase is likely due to a requirement for clathrin in Weibel-Palade body maturation, such that vWF is shunted to the constitutive pathway upon clathrin blockade [55]. vWF secretion was not significantly impacted by dynamin blockade via dynasore treatment (Fig. 3K, Suppl. Fig. 3I). vWF secretion was also unaffected by the blockade of SNAREs with TATNSF700 which reduced sFLT1 secretion (Fig. 3L, Suppl. Fig. 3J), and cholesterol depletion via β-methyl-cyclodextrin elevated constitutively secreted vWF levels while not affecting sFLT1 secretion (Fig. 3M, Suppl. Fig. 3K). Thus, although sFLT1 and constitutive vWF secretion both depend on Golgi transport and lysosomal degradation, the divergent sensitivity profiles indicate that sFLT1 and vWF utilize different trafficking pathways to move from the Golgi to the plasma membrane for constitutive secretion from endothelial cells.

Intracellular sFLT1 is mis-localized following trafficking perturbations

To precisely define effects of pharmacological blockade on sFLT1 trafficking, we used immunofluorescence imaging to determine changes in sFLT1 intracellular localization. Brefeldin-A treatment that disrupts the Golgi and blocked sFLT1 secretion resulted in mis-localization of both sFLT1-HA and endogenous FLT1 signal from the Golgi to the ER [Fig. 4A(a, b) and B(a, b)], consistent with previous findings [69]. Blockade of clathrin assembly through chlorpromazine treatment also inhibited sFLT1 secretion, and this manipulation increased both sFLT1-HA and FLT1 intensity within the Golgi and in large perinuclear puncta compared to controls [Fig. 4A(a, c), B(a, c)], consistent with clathrin being required for sFLT1 trafficking from the Golgi. Although TATNSF700 inhibited sFLT1 secretion, it did not affect sFLT1-HA or FLT1 localization [Fig. 4A(a, d) and B(a, d)], perhaps because unsynchronized constitutive vesicle movement in the cytoplasm is below the sensitivity of detection. Finally, after inhibition of lysosomal degradation with chloroquine treatment, sFLT1-HA and endogenous FLT1 reactivity became more pronounced in large puncta surrounding the Golgi [Fig. 4A(a, e) and B(a, e)], consistent with intracellular accumulation in the absence of degradation. Overall, intracellular sFLT1 localization had a similar sensitivity profile to sFLT1 secretion following pharmacological

manipulations, and both revealed an unexpected requirement for clathrin at the Golgi-to-vesicle step of trafficking of sFLT1 in endothelial cells.

sFLT1 in polarized vessels and in vivo is sensitive to clathrin inhibition

Since trafficking dynamics in vivo occur in a 3D environment, we assessed sFLT1 intracellular localization following pharmacological trafficking manipulations in polarized blood vessels. Using a 3D sprouting angiogenesis assay that results in lumenized and polarized endothelial cell sprouts [92, 93], FLT1 signal was detected in the Golgi of control HUVEC sprouts [Fig. 5A(a)], and FLT1 in endothelial cell sprouts displayed similar localization changes following inhibitor treatments as seen in 2D culture. FLT1 became diffuse and ER-localized following brefeldin-A treatment [Fig. 5A(b)], while treatment with either chlorpromazine to block clathrin assembly or chloroquine to block lysosomal degradation resulted in FLT1 accumulation in the Golgi and perinuclear puncta [Fig. 5A(c, d)]. These data are consistent with a requirement for Golgi trafficking, clathrin, and lysosomal degradation in the proper localization of intracellular FLT1 in polarized vessels.

To assess the unique requirement of clathrin for sFLT1 localization in polarized vessels in vivo, Tg(fli1a:LifeAct-GFP)^{mu240} zebrafish embryos were micro-injected with a tagged sflt1 construct, flt1^{enh}:sflt1_Δ7-HAHA, at the one-cell stage and analyzed at 32 h post-fertilization (hpf). Overexpression of wild-type sflt1 in zebrafish is lethal, so a construct containing a short deletion in the VEGF-binding domain predicted to prevent VEGF binding and tolerated by fish embryos was used [94]. Mosaic expression of sflt1_Δ7-HAHA was detected in the dorsal aorta and arterial intersegmental vessels of the trunk, using an HA antibody and a mask of Tg(fli1a:LifeAct-GFP)^{mu240} over the DAPI nuclear signal to visualize endothelial cell nuclei (Fig. 5B, a). Under control conditions, HA signal localized to the perinuclear space of endothelial cells. Chlorpromazine treatment to block clathrin resulted in HA signal accumulation around the nuclei of zebrafish endothelial cells, similar to the pattern seen in vitro with these manipulations (Fig. 5B, b).

We next investigated clathrin-dependent endogenous zebrafish flt1 localization using a transgenic line with a HA-tag inserted into the flt1 locus, TgTm(flt1_E3_HAHA)^{ka611} line [94]. HA antibody staining in the dorsal aorta and arterial intersegmental vessels of 32 hpf TgTm(flt1_E3_HAHA); Tg(fli1a:LifeAct-GFP) embryos was largely perinuclear in controls (Fig. 5C, a). Consistent with the HUVEC results and sflt1_Δ7-HAHA embryos, HA signal accumulated throughout the cell following chlorpromazine treatment (Fig. 5C, b). Overall, sFLT1 localization and sensitivity profiles in 2D cultures were similar in 3D polarized vessels

Fig. 4 Intracellular sFLT1 is mis-localized following trafficking perturbations. **A**(a–e); **B**(a–e) HUVEC immunofluorescence stained for sFLT1-HA (**A**(a–e)) or FLT1 (**B**(a–e)), GM130 (Golgi), and DAPI (nucleus) after 4 h of indicated pharmacological inhibitor treatments. n = 3 replicates. Scale bars, 10 μm. Yellow arrows: Golgi-localized sFLT1-HA (**A**) or FLT1 (**B**); pink arrowheads: sFLT1-HA (**A**) or FLT1 (**B**) localized to puncta
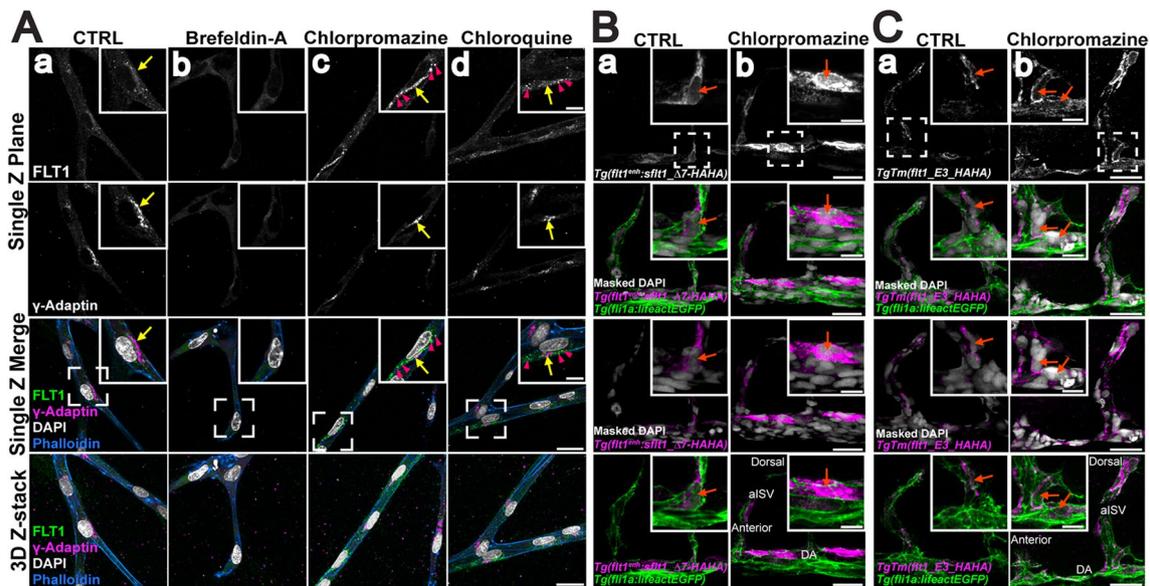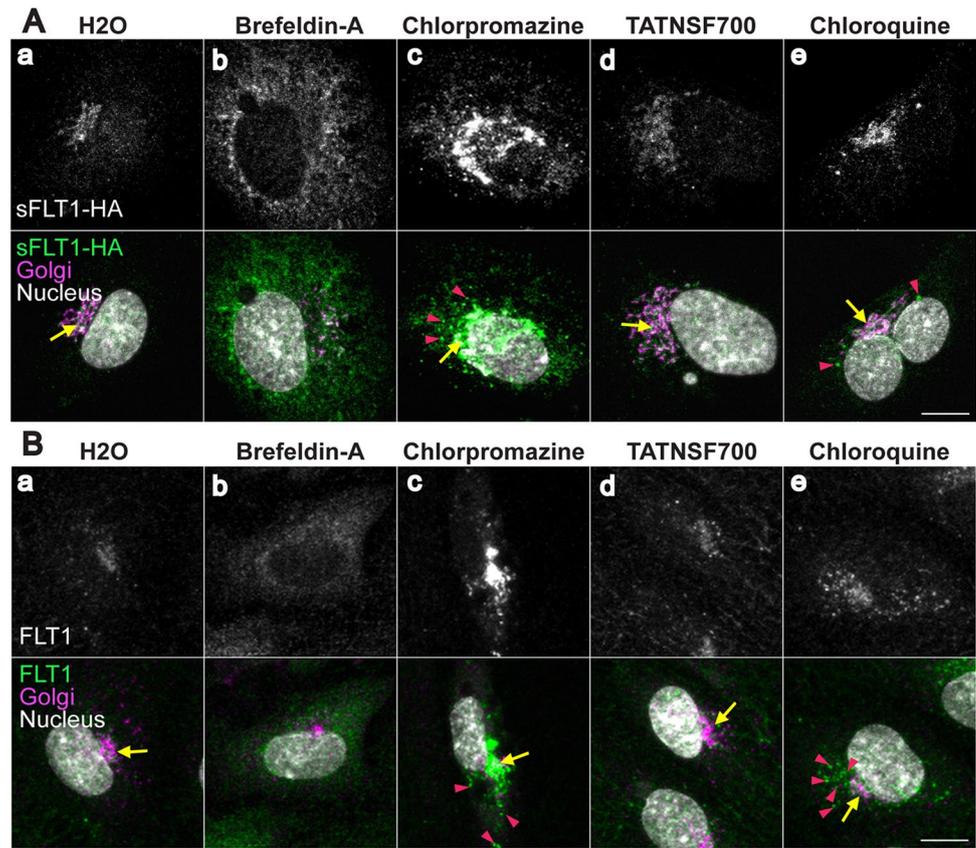

Fig. 5 sFLT1 localization in polarized vessels and in vivo is sensitive to trafficking perturbations. **A**(a–d) Single Z-plane and 3D Z-stack of representative images of day 7 3D HUVEC sprouting assay with indicated inhibitor treatments (18 h) and stained for FLT1, γ-Adaptin (Golgi), DAPI (nucleus), and phalloidin (actin). Scale bar, 25 μm; inset from dashed region scale bar: 10 μm. n = 3 replicates, 5 beads per condition per replicate. Yellow arrows: Golgi-localized FLT1; pink arrowheads: FLT1 localized to puncta. **B**(a, b) Immunofluorescence of 32 hpf *Tg(flt1^{enh}:sFLT1_Δ7-HAHA)^{ka612}*; *Tg(fl1ai:lifeactE*-*GFP)^{mu240}* zebrafish embryos labeled with HA antibody and masked DAPI following 6 h of chlorpromazine treatment. orange arrows: nucleus. Scale bar, 25 μm; inset from dashed region scale bar: 10 μm. n = 3 replicates. **C**(a, b) Representative images of 32 hpf *TgTm(flt1_E3_HAHA)^{ka611}*; *Tg(fl1ai:lifeactEGFP)^{mu240}* zebrafish embryos labeled with HA antibody and masked DAPI following 6 h of chlorpromazine treatment. Scale bar, 25 μm; inset from dashed region scale bar: 10 μm. n = 3 replicates. orange arrows: nucleus. *DA* dorsal aorta, *aISV* arterial intersegmental vessel

in vitro and in vivo, and clathrin blockade mis-localized sFLT1 and blocked secretion in 2D culture as well as in polarized vessels, indicating similar requirements for sFLT1 trafficking in physiologically relevant topologies.

Endothelial sFLT1 secretion requires RAB27a and SNAREs

Some post-Golgi proteins are directly targeted to the plasma membrane, while others fuse with storage granules, recycling endosomes, or other intermediates prior to plasma membrane docking and secretion [42, 95, 96]. To define a molecular pathway for sFLT1 trafficking/secretion in endothelial cells, we used siRNA-mediated depletion in primary endothelial cells to target specific trafficking components. Due to the technical challenges of studying small, fast-moving vesicles, the molecular components of constitutive secretion are not well-defined. However, several RABs and SNAREs that localize to recycling endosomes or storage granules in endothelial cells have been identified [97–99], and the RAB GTPase RAB27a is required to transport and dock Weibel-Palade bodies in endothelial cells for stimulated secretion of vWF [100, 101]. We found that RAB27a silencing significantly blocked constitutive sFLT1 secretion without significant reduction of internal sFLT1 levels (Fig. 6A, Suppl. Fig. 4A, C). In contrast, depletion of the recycling endosome-localized RABs RAB4a, RAB11a, or RAB8a did not significantly affect sFLT1 secretion or internal sFLT1 levels compared to non-targeting controls (Fig. 6A, Suppl. Fig. 4A, D–F). Therefore, endothelial cell post-Golgi transport of sFLT1 to the plasma membrane requires RAB27a but not RABs associated with recycling endosomes, suggesting that sFLT1 trafficking requirements overlap with requirements for granule formation and Weibel-Palade body transport.

Fusion of Golgi-derived vesicles with recycling endosomes, storage granules, and the plasma membrane requires SNARE complex formation [48]. The functional SNARE inhibitor, TATNSF700, blocked sFLT1 secretion from endothelial cells; therefore, a panel of endothelial SNAREs was analyzed to determine specificity in sFLT1 trafficking. The SNAREs SNAP23, STX3, STX4, VAMP3, and VAMP8 promote fusion of Weibel-Palade bodies with the plasma membrane for stimulated secretion of vWF, and STX6 mediates trans-Golgi vesicle trafficking events including localization to clathrin-coated membranes and recycling endosomes [59, 60, 102–105]. Depletion of STX6, STX3 or VAMP3 significantly blocked sFLT1 secretion while si*SNAP23*, si*VAMP8*, and si*STX4* treatment did not affect sFLT1 secretion (Fig. 6B, Suppl. Fig. 4G–K). Internal sFLT1 levels did not significantly change relative to controls after SNARE depletions (Suppl. Fig. 4B). Consistent with this profile, density

gradient fractionation revealed that RAB27a, VAMP3 and STX3 were co-localized with sFLT1 in fractions that likely contained vesicles, as defined by their density, presence of Rab27A, and lack of STX6. In contrast, RAB4 that is associated with recycling at the membrane did not co-localize with sFLT1 (Fig. 6C). Together, these data indicate that RAB27a, VAMP3, STX3, and STX6 are required for sFLT1 secretion from endothelial cells. We compared sFLT1 requirements for RAB27a, STX6, STX3, and VAMP3 for endothelial cell secretion to requirements for constitutive vWF secretion, and we found that unlike stimulated release of vWF through Weibel-Palade bodies, constitutive vWF secretion was not significantly changed by depletion of any of the RABs or SNAREs tested compared to controls (Fig. 6D, E), consistent with published work.

Trans-Golgi trafficking is required for angiogenic sprouting

Trans-Golgi trafficking is the rate-limiting step of constitutive secretion [83]; therefore, we further analyzed the relationship of intracellular sFLT1 and trans-Golgi localized STX6. Immunofluorescence localization in HUVEC revealed that sFLT1-HA and FLT1 colocalized with STX6 at the Golgi under control conditions (Fig. 7A, A′ and B, B′) and remained Golgi-localized upon STX6 depletion, although FLT1 antibody signal was reduced in endothelial cells silenced for STX6 (Fig. 7C, D). FLT1 loss or reduction increases angiogenic sprouting in vitro and in vivo [18, 39, 40, 70, 106, 107], consistent with its function as a negative regulator of VEGF-A signaling. To test if STX6-mediated trans-Golgi trafficking impacts angiogenic sprouting, we subjected STX6-depleted HUVEC to the 3D sprouting assay. We confirmed that depletion of either total FLT1 (both mFLT1 and sFLT1) or only sFLT1 led to increased endothelial sprouting, with significantly increased sprout numbers and total vessel area (Fig. 7E–G, I–J). STX6 depletion phenocopied the increased sprouting parameters (Fig. 7H–J), consistent with the idea that disrupting the critical Golgi-to-vesicle step of sFLT1 secretion from endothelial cells contributes to angiogenic sprouting defects. However, STX6 depleted sprouts appeared narrower and less branched than sprouts depleted for sFLT1, perhaps because STX6 also functions in VEGFR2 and integrin trafficking that may impact blood vessel sprouting [103, 108].

Golgi-to-vesicle sorting of sFLT1 is mediated by AP1

We further evaluated the role of Golgi trafficking in sFLT1 secretion by depleting Golgi-localized trafficking proteins or their plasma membrane-localized counterparts and assessing effects on sFLT1 secretion and intracellular localization.

Fig. 6 sFLT1 trafficking requires RAB27a and SNAREs. Quantification of sFLT1 (**A**, **B**) or vWF (**D**, **E**) immunoblot band intensity in 18 h HUVEC concentrated media following indicated RAB (**A**, **D**) or SNARE (**B**, **E**) siRNA treatments normalized to siNT. Statistics: Mean +/− SD per experiment. One-way ANOVA with pairwise comparison and post-hoc Tukey's range test. *$P < 0.05$, **$P < 0.01$, ***$P < 0.001$, ns, not significant. **C** HUVEC density ultracentrifugation subcellular fractionation probed for RABs and SNAREs in sFLT1-containing fractions. Other markers: Calnexin (ER); ZO1 (plasma membrane); GAPDH (cytosol)
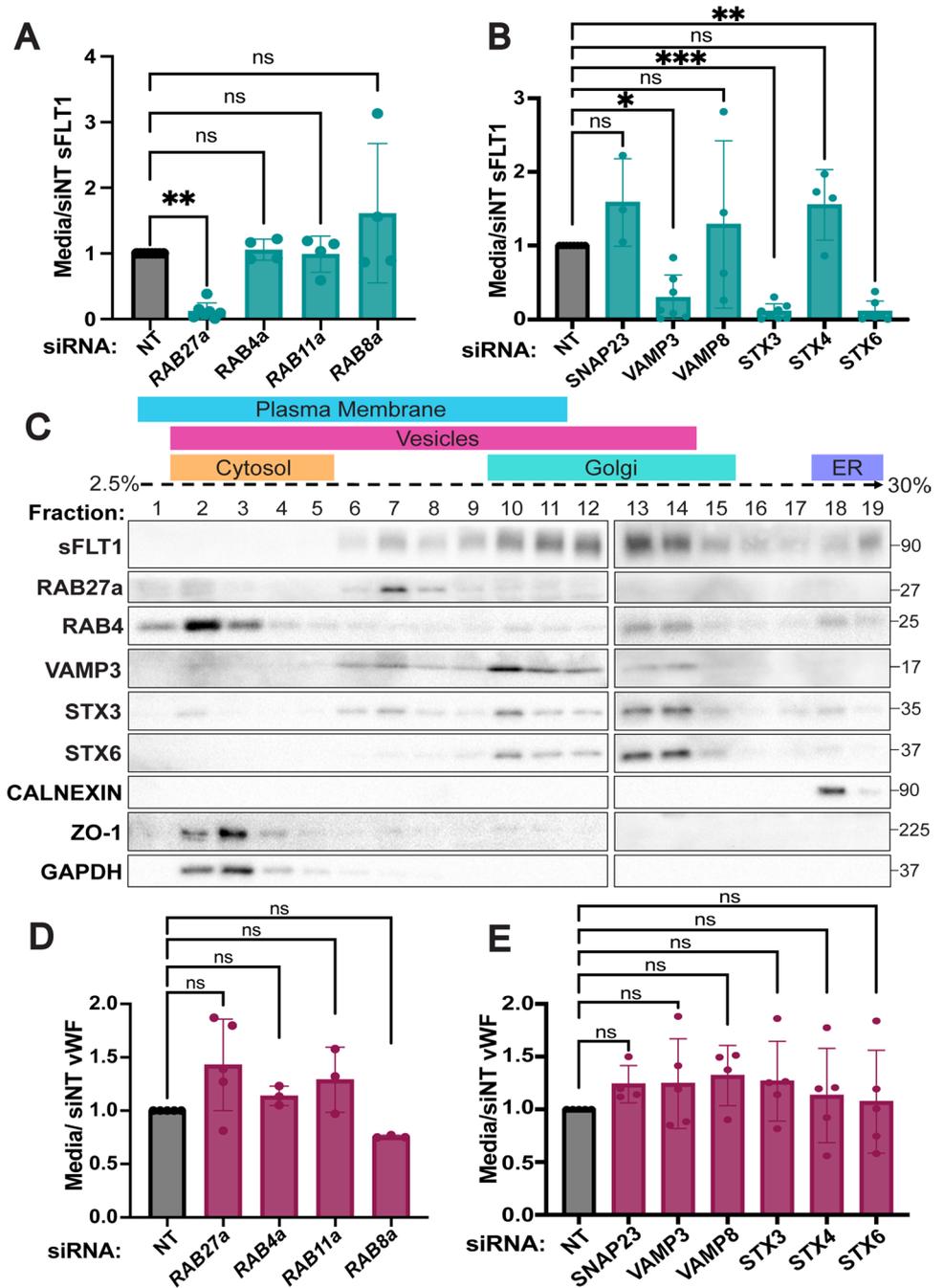
ARF1, a downstream target of brefeldin-A, is required at the Golgi to recruit COPI coated vesicle proteins and clathrin adaptors such as AP1 [109]. In contrast, ARF6 assists in rearranging actin near the plasma membrane [109]. HUVEC were treated with siRNAs targeting ARF1 or ARF6, and si*ARF1* blocked accumulation of sFLT1 in the media compared to controls without affecting sFLT1 levels internally (Fig. 8A, Suppl. Fig. 5 A, D), whereas ARF6 depletion did not alter secreted or intracellular sFLT1 levels (Fig. 8B,

Suppl. Fig. 4B, E). These findings indicate that Golgi-localized ARF1 regulates sFLT1 secretion while peripheral ARF6 does not affect secretion.

To determine whether the unexpected clathrin requirement for sFLT1 secretion was linked to the Golgi, we depleted the μ1 subunit of the Golgi-localized adaptor protein, AP1 (si*AP1M1*), or the α1 subunit of plasma membrane-localized AP2 (si*AP2A1*) [85], as complexes with each subunit are predicted to promote clathrin-dependent
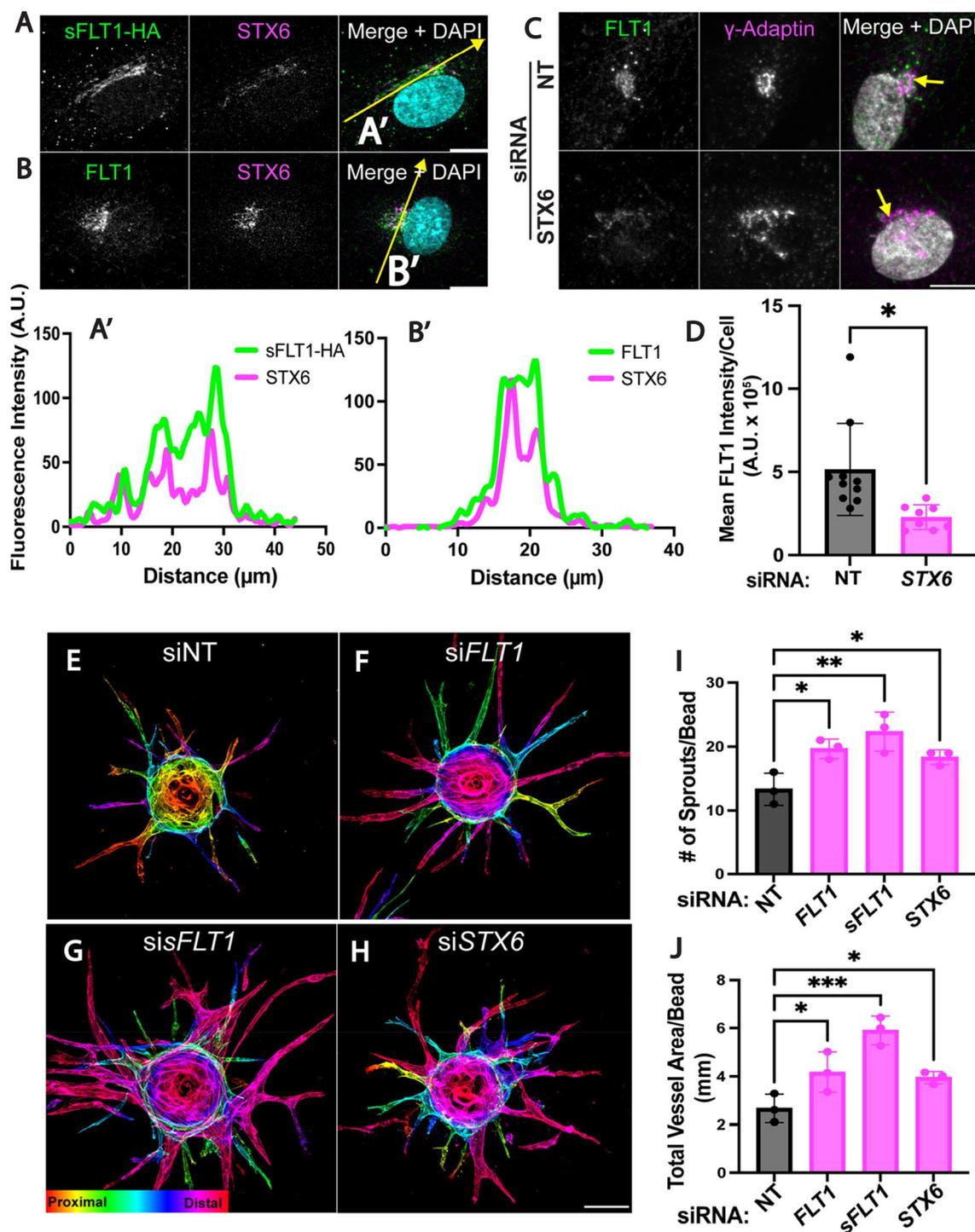
Fig. 7 STX6 co-localizes with sFLT1 and regulates angiogenic sprouting. **A**, **B** HUVEC immunofluorescence imaging of sFLT1-HA (**A**) or FLT1 (**B**) and STX6 and DAPI. Scale bar, 20 μm. Yellow line, line scan. **A′–B′** Line scan analysis of sFLT1-HA (**A′**) or FLT1 (**B′**) and STX6 fluorescence intensity. **C** Representative immunofluorescence staining of FLT1, γ-adaptin, and DAPI in HUVEC transfected si*STX6* or siNT. Scale bar, 10 μm. **D** Mean FLT1 intensity analysis/cell of HUVEC transfected si*STX6* or siNT. Statistics: mean +/− SD of FLT1 intensity/nucleus, n = 3 replicates, students two-tailed *t*-test.

*P < 0.05. **E–H** Immunofluorescence imaging of 3D HUVEC following indicated siRNA transfections and 4 days of sprouting. Phalloidin staining depth encoded. Scale bar: 100 μm. n = 3 replicates, 3 beads per replicate. **I** Quantification of sprout number/bead. **J** Quantification of the total vessel area/bead (μm). Statistics: mean +/− SD of 3 beads/experiment, n = 3 replicates, one-way ANOVA with pairwise comparison and post-hoc Tukey's range test. *P < 0.05, **P < 0.01, ***P < 0.001

Fig. 8 Golgi trafficking of sFLT1 is clathrin-mediated. **A–D** Quantification of sFLT1 immunoblot band intensity in HUVEC conditioned media with indicated siRNA treatments normalized to siNT. **E** Immunofluorescence staining of sFLT1-HA and clathrin and DAPI in HUVEC transfected with si*AP1M1* or siNT. Representative of n = 3 replicates. Scale bar, 10 μm. **F** Quantification of clathrin intensity in sFLT1-HA area, n = 3 replicates, **G–J** Quantification of vWF immunoblot band intensity in HUVEC conditioned media with indicated siRNA treatments normalized to siNT. Statistics: Mean +/− SD of experimental replicates shown. students two-tailed *t*-test. *P < 0.05, **P < 0.01, *ns* not significant
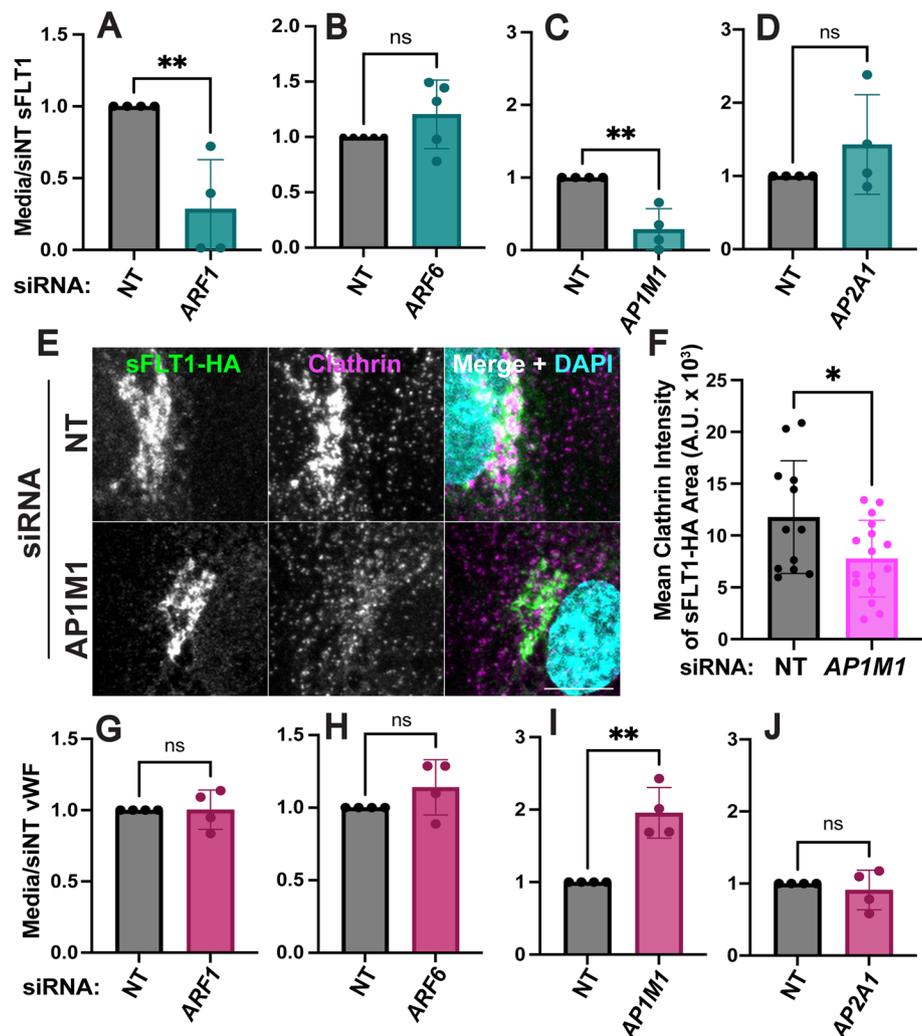
trafficking at different cellular locations. sFLT1 secretion was inhibited by si*AP1M1* but not si*AP2A1*, indicating that clathrin-dependent sFLT1-trafficking likely occurs at the Golgi but not the plasma membrane (Fig. 8C, D, Suppl. Fig. 5F, G). As described earlier, sFLT1-HA and FLT1 colocalize with the gamma subunit of AP1, γ-Adaptin, in the Golgi; internal sFLT1 levels were reduced after si*AP1M1* but not si*AP2A1* treatment compared to controls (Suppl. Fig. 5C, F, G). Immunofluorescence imaging of sFLT1-HA revealed that AP1M1 depletion reduced clathrin intensity within the Golgi-localized sFLT1-HA area (Fig. 8E, F). Therefore, sFLT1 likely requires clathrin-dependent sorting at or near the Golgi for secretion.

Together, these findings establish a requirement for ARF1 and AP1 at the Golgi for proper trafficking and secretion of constitutive sFLT1. To determine if constitutive vWF also exhibits these requirements in endothelial cells, we interrogated constitutive vWF secretion in parallel. Neither ARF1 nor ARF6 depletion affected accumulation of constitutive

vWF in the media (Fig. 8G, H). Constitutive vWF secretion significantly increased following AP1M1 depletion and did not change with AP2A1 depletion (Fig. 8I, J), consistent with published work [55]. Therefore, sFLT1 trafficking in endothelial cells diverges from constitutive vWF trafficking in the same cells at or near the Golgi.

Regulated ER release of sFLT1 reveals clathrin-dependent vesicle trafficking in endothelial cells

Constitutive secretion is unsynchronized and highly dynamic, making post-Golgi vesicle trafficking difficult to visualize. To capture the dynamics of sFLT1 trafficking in endothelial cells, we utilized a previously validated Retention Using Selective Hook (RUSH) assay designed to hold tagged proteins in the ER prior to regulated release via addition of biotin [110–112]. Tagged sFLT1 (sFLT1-SBP-EGFP) was expressed in HUVEC (Fig. 9A; Suppl. Fig. 6A, B), and

time-lapse imaging with temporal projection showed tagged sFLT1 movement from the ER to the Golgi 15 min post-biotin (Fig. 9B, C; Suppl. Movie 1). At 30 min post-biotin, labeled vesicles became visible as they moved from the Golgi to the plasma membrane, and by 45 min post-biotin, tagged sFLT1 signal began to diminish, presumably due to secretion (Fig. 9B, C; Suppl. Movie 1). This live-image data supports that sFLT1 traffics from the Golgi to the plasma membrane via vesicles. More precise localization of tagged sFLT1 at 30 min post-biotin, when vesicles begin to exit the Golgi, showed that tagged sFLT1 colocalized with the trans-Golgi marker, Golgin-97 (Suppl. Fig. 6C–C′). High resolution imaging revealed co-localization of tagged sFLT1 with clathrin staining near the Golgi (Fig. 9D–D′), consistent with a role for clathrin in the sorting of sFLT1 into vesicles. Moreover, vesicles positive for tagged sFLT1 were present in VE-cadherin positive areas at the cell periphery at this time, suggesting movement to the plasma membrane near cell-cell junctions (Fig. 9E–E′).

To functionally assess the clathrin-dependence of sFLT1 trafficking in this system, HUVEC expressing tagged sFLT1 were subjected to pharmacological blockade of clathrin assembly, and significantly fewer tagged sFLT1 vesicles were detected in treated cells compared to controls 30 min post-biotin (Fig. 9F, G). Live-cell trafficking dynamics were next compared, and vesicles began trafficking on average 30 min post-biotin in controls, with the intracellular intensity of tagged sFLT1 steadily decreasing over time (Suppl. Movie 2). In contrast, with clathrin blockade 54% (7/13) imaged cells lacked detectable vesicles during this time compared to 10% (1/10) of controls (Fig. 9H). Of the clathrin-blocked cells that produced vesicles, the vesicles appeared with a significant time delay (Fig. 9I; Suppl. Movie 3). Therefore, synchronizing sFLT1 secretion from endothelial cells supports that sFLT1 undergoes clathrin-dependent sorting at or near the Golgi prior to entry into constitutively secreted vesicles for trafficking to the plasma membrane.

Discussion

Here we define a unique trafficking pathway for endothelial cell secretion of sFLT1 (Fig. 10), a critical regulator of VEGF-A signaling involved in blood vessel formation and vascular pathologies. Constitutive sFLT1 secretion utilizes STX6, ARF1, and AP1-dependent clathrin at or near the Golgi, likely for sorting into vesicles for trafficking to the plasma membrane via RAB27a and specific SNAREs. Blockade or depletion of trafficking/secretion components led to sFLT1 mis-localization within endothelial cells, in polarized 3D vessels, and in vivo in zebrafish. Thus, our findings highlight the importance of sFLT1 trafficking and

secretion in the regulation of blood vessel formation and provide new targets for pathway regulation.

We used computational modeling to predict a sFLT1 secretion rate of approximately 30,000 molecules/cell/hr, which is well in excess of what is likely needed to create significant reservoirs of interstitial sFLT1 in tissues [113]. Notably, our estimated endothelial sFLT1 secretion rate is also higher than the secretion rate of the ligand VEGF-A from stromal cells (~ 250–1250 molecules/cell/hr) [73]. This implies that in most well-vascularized tissues, interstitial sFLT1 levels are predicted to exceed those of VEGF-A, consistent with a role for sFLT1 in modulating VEGF-A signaling and regulating angiogenesis. Our mechanistic model parameters are consistent with sFLT1 secretion time courses across 3 independent studies, and further modeling of blockade effects was consistent with experimental data, suggesting that this model will be useful in the future to determine how individual processes contribute to sFLT1 secretion and to simulate mechanistic interventions.

Of the main routes for protein trafficking from the Golgi to the cell surface [42, 95, 96], our data supports a model whereby most endothelial sFLT1 is secreted via clathrin-dependent intermediate sorting prior to vesicle trafficking. Although we cannot rule out that some sFLT1 is also secreted via small unregulated vesicles, disruption of the clathrin-mediated pathway via pharmacological blockade or depletion of clathrin-associated components did not lead to rescue of sFLT1 secretion by alternate trafficking routes, and regulated release of tagged sFLT1 supported a role for clathrin-mediated sorting in vesicle transport to the plasma membrane. Although clathrin-mediated trafficking is linked to recycling from the plasma membrane via endosomes [81], we found no evidence that sFLT1 secretion utilizes traditional surface-endosomal recycling trafficking proteins (i.e. ARF6, RAB4, RAB11, RAB8, AP2), consistent with the idea that secreted proteins are usually not recycled from the cell surface. A previous study linked trafficking of stably overexpressed sFLT1 to ARF6 and RAB11 [69], perhaps due to different expression modalities. The intermediate sorting pathway for sFLT1 secretion described here depends on AP1. AP1-mediated clathrin assembly is required for the maturation of immature Golgi-derived secretory granules in many cell types, including endothelial cells [51, 55], and AP1 works with clathrin to sort uncondensed proteins for trafficking as they condense into secretory granules, likely to target lysosomes or the plasma membrane [50]. Proteins trafficked via this mechanism include lysosomal enzymes that interact with mannose-6-phosphate receptors for lysosomal sorting, and proinsulin that is sorted from condensed insulin into immature granules for constitutive secretion [50, 52, 114].
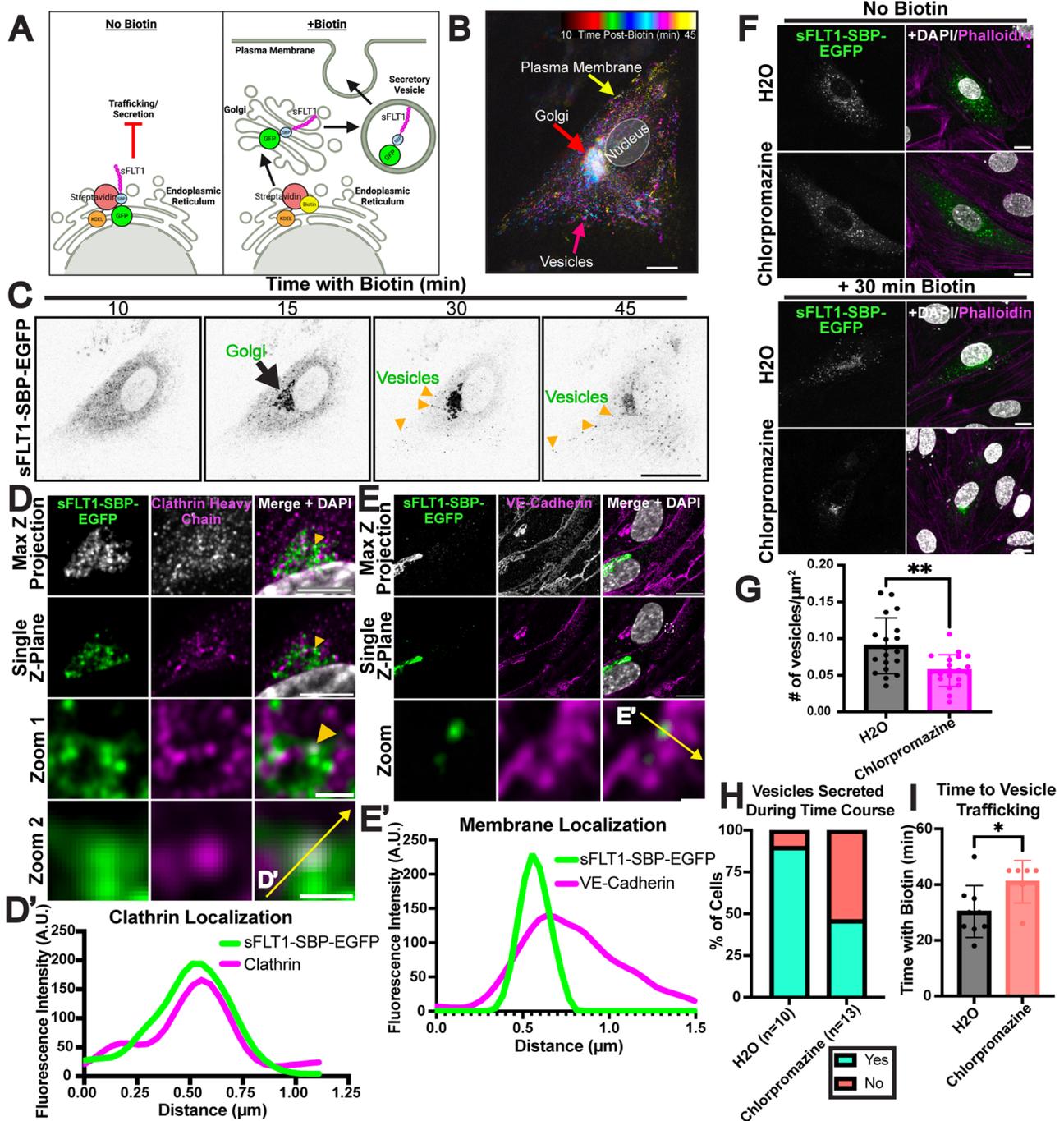
Evidence that sFLT1 trafficking utilizes intermediate sorting is also supported by our finding that STX6 is required for sFLT1 secretion, since STX6 colocalizes with AP1/clathrin on immature granules and regulates Golgi-to-vesicle transport [52–54]. Moreover, our finding that sFLT1 and STX6 partially colocalize through cell fractionation and immunofluorescence imaging suggests a requirement for STX6 in the trafficking of sFLT1 from the Golgi. Thus, our findings are consistent with a model whereby newly synthesized sFLT1 utilizes immature granule-like sorting into vesicles

for secretion (Fig. 10). Blockade of clathrin assembly in sprouting endothelial cells in vitro and in zebrafish revealed sFLT1 mis-localization as seen in 2D culture, and depletion of STX6 largely phenocopied FLT1 depletion in sprouting parameters, leading to excess sprouting, consistent with the idea that Golgi trafficking and secretion of sFLT1 is operative in physiologically relevant settings.

We compared endothelial cell sFLT1 trafficking/secretion requirements to those of vWF, as the stimulated endothelial vWF trafficking pathway is well described [61, 62, 105,

◄**Fig. 9** Regulated release of sFLT1 in endothelial cells reveals clathrin-dependence. **A** Diagram of sFLT1 trafficking by the Retention Using Selective Hooks (RUSH) assay. Created with Biorender.com. **B** Temporal projection of tagged sFLT1 (sFLT1-SBP-EGFP) expressing HUVEC 10–45 min post-biotin addition. Tagged sFLT1 moves to the Golgi (red arrow), then into vesicles (pink arrow) that localize near the plasma membrane (yellow arrow). **C** Panels of tagged sFLT1-expressing HUVEC post-biotin and live-imaged at indicated times (min). **D** Airyscan immunofluorescence imaging of tagged sFLT1 (green) HUVEC with clathrin antibody (magenta) and DAPI (white) stain 30 min post-biotin addition. Scale bar, 10 μm. Zoom 1 scale bar, 1 μm. Zoom 2 scale bar, 0.5 μm. Yellow arrow, colocalization of tagged sFLT1 and clathrin near Golgi exit sites. Yellow line, line scan. **D′** Line scan of tagged sFLT1 and clathrin intensity in single Z plane. **E** Airyscan immunofluorescence imaging of tagged sFLT1-expressing HUVEC with VE-Cadherin (magenta) and DAPI (white) 30 min post-biotin. Scale bar, 10 μm. Zoom from dashed region scale bar, 0.5 μm. Yellow line, line scan. **E′** Line scan of tagged sFLT1 and VE-Cadherin intensity in single Z plane. **F** Immunofluorescence staining of control or 6 h chlorpromazine-treated tagged sFLT1 + HUVEC with DAPI and phalloidin (F-actin) +/− 30 min incubation with biotin. Scale bar, 10 μm. **G** Quantification of tagged sFLT1 + vesicles/cell area ($μm^2$) in control or chlorpromazine treated HUVEC 30 min post-biotin addition, n = 4 replicates. **H** Quantification of % of control or chlorpromazine treated tagged sFLT1 HUVEC with vesicles within 60 min of biotin incubation during time-lapse imaging. **I** Time post-biotin addition (min) for tagged vesicle secretion detection during time-lapse imaging. Cells with no vesicles excluded. n = 5 replicates. Statistics: Mean +/− SD of experimental replicates shown. Students two-tailed *t*-test. *P < 0.05, **P < 0.01

115]. Interestingly, despite being constitutively secreted like unstimulated vWF, sFLT1 utilizes some trafficking components also used for stimulated vWF secretion via Weibel-Palade bodies. AP1-mediated clathrin assembly in constitutive sFLT1 secretion described here is similar to requirements for Weibel-Palade body maturation [55], although this requirement is not shared by constitutive vWF secretion assayed in parallel. RAB27a, VAMP3, and STX3 are required for constitutive sFLT1 secretion and for histamine-responsive Weibel-Palade body release but not constitutive vWF secretion [58]. However, sFLT1 is not detectable in mature Weibel-Palade bodies [63], and unlike vWF secreted by Weibel-Palade bodies, sFLT1 secretion depends on the SNARE STX6 but not SNAP23, STX4, or VAMP8. Thus, some trafficking components appear to be shared while others differ between constitutive and stimulated pathways for secretion from endothelial cells, setting up a unique "hybrid" clathrin-dependent trafficking pathway for endothelial sFLT1 secretion.

sFLT1 secretion from endothelial cells is critical to its regulation of VEGF signaling, and our findings reveal novel aspects of sFLT1 trafficking and secretion that define a unique pathway for sFLT1 constitutive trafficking/secretion from endothelial cells. The importance of secreted sFLT1 in vascular function is highlighted by recent work showing that vascular decline is linked to endothelial cell aging

and reduced microvascular density, and that these changes are in turn promoted by reduced VEGF signaling resulting from elevated sFLT1 serum levels [24]. It is possible that trafficking/secretion of the soluble FLT1 isoform contributes to increased serum levels of sFLT1 and age-related endothelial cell dysfunction, along with changes in alternative splicing of FLT1 described in the study. Since vascular decline is thought to be a major driver of numerous age-related changes in metabolism and inflammatory responses, the regulation of sFLT1 secretion likely has a central role in maintaining homeostasis throughout life.

Materials and methods

Cell culture

Human umbilical vein endothelial cells (HUVEC) (Lonza, #C2519A, Lot # 0000636513, 0000661173 and 0000704189) were cultured in EBM-2 media supplemented with a bullet kit (EGM-2) (Lonza, #CC-1362) and 1x antibiotic-antimycotic (Gibco). HUVEC were used from passages 3–6. Normal human lung fibroblasts (NHLF) (Lonza, #CC-2512) were cultured in DMEM (Gibco, #11,965,118)
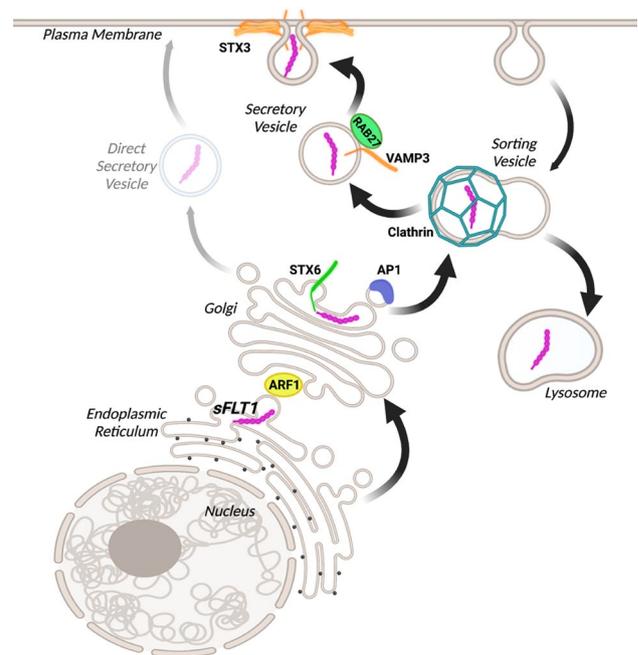

Fig. 10 Model for sFLT1 trafficking and secretion from endothelial cells. The data is consistent with a model whereby sFLT1 is trafficked between the endoplasmic reticulum and Golgi by ARF1, the Golgi and a clathrin-coated sorting compartment by STX6 and AP1, and finally through constitutive vesicles to the plasma membrane by RAB27a, VAMP3, and STX3 or to the lysosome for degradation. An additional direct secretory pathway from the Golgi may be utilized although it does not compensate for the loss of the depicted trafficking components. Figure made with Biorender.com

supplemented with 10% fetal bovine serum (FBS) and 1× antibiotic-antimycotic (Gibco) and used at passages 4–10. HEK293T/17 (ATCC #CRL-11268) were maintained in DMEM supplemented with 10% FBS and 1× antibiotic-antimycotic and used at passages 6–12. All cells were maintained at 37 °C and 5% CO_2. HUVEC, NHLF, and HEK193T/17 cells were certified mycoplasma-free by the UNC Tissue Culture Facility.

Inhibitor treatments

For secretion experiments, HUVEC were grown to 80% confluency, washed with PBS, then incubated in Fibroblast Basal Media (Lonza, #CC-3131):EGM-2 (1:1, FBM/EGM) containing pharmacological inhibitors (Suppl. Table S6) or vehicle controls for 18 h at 37 °C before protein collection. For trafficking experiments, HUVEC were allowed to adhere overnight at 37 °C, then FBM/EGM with inhibitors or controls was added for 4 h at 37 °C before fixation.

Plasmid expression

The human sFLT1-HA plasmid construct was created through Gibson cloning of human sFLT1 cDNA into a pcDNA3.1 vector containing a C-terminal HA tag (pcDNA3-ALK2-HA, a gift from Aristidis Moustakas (Addgene plasmid #80870)) [116]. The Retention Using Selective Hooks (RUSH) construct, Str-KDEL_sFLT1-SBP-EGFP, was created by replacing TNF in Str-KDEL_TNF-SBP-EGFP (a gift from Franck Perez (Addgene plasmid #65278)) with sFLT1 from sFLT1-HA using Gibson cloning [110]. Sequencing validation was performed through Genewiz.

For sFLT1-HA expression in HUVEC, cells were grown to 95% confluency, trypsinized in 0.05% Trypsin-EDTA (Gibco, #25300-054) at 37 °C for 3 min, then collected in 1:1 sterile PBS/new born calf serum (NBCS) (Gibco, #16010-159). Cells were pelleted at 1000 rpm for 5 min and resuspended in 100 μL nucleofector solution (Lonza, #VPB-1002) before adding 2.5 μg of plasmid. The suspension was electroporated into cells using the Amaxa Nucleofector System (D-005 program), and cells were then resuspended and seeded in fresh EGM-2. The cells were left to adhere for 6 h at 37 °C and 5% CO_2 before adding secretion media (1:1 FBM/EGM) to allow for overnight recovery and to remove dead cells. 24 h after electroporation, the samples were either fixed with 4% PFA for IF or collected for western analysis.

HEK293T/17 sFLT1-HA expression and HUVEC Str-KDEL_sFLT1-SBP-EGFP expression followed a similar protocol except cells were incubated in media with 2.5 μg plasmid diluted in 1 mL OptiMem (Gibco, #11058021) with 15 μL Lipofectamine 3000 + 15 μL P3000 reagent (ThermoFisher, #L3000015) according to manufacturer's protocol

for 24 h at 37 °C. 24 h post-transfection, cells were pelleted and re-seeded for analysis the following day.

siRNA transfection

HUVEC were grown to 75–80% confluency and incubated in EGM-2 with 200 pmol siRNAs (Suppl. Table S7) diluted in 1 mL OptiMem and 20 μL Lipofectamine 3000 (ThermoFisher, #L3000015) according to manufacturer's protocol for 24 h at 37 °C. Cells were pelleted, resuspended in EGM-2, and added to fibronectin-coated culture slides for staining or plates for protein collection. 48 h post-transfection, secretion media (1:1 FBM/EGM) was added. 72 h post-transfection, media was collected and cells were either fixed with 4% PFA for IF or collected for western analysis.

Protein collection and western blots

Conditioned media was collected [61], then cells were lysed in 100–200 μL RIPA buffer containing 1X protease-phosphatase inhibitor cocktail (Cell Signaling, #5872S), as previously described [107]. Conditioned media was centrifuged for 5 min at 2500×g at 4 °C to pellet remaining cells, then concentrated (Amicon, #UFC803024) per manufacturer's protocol and centrifuged for 10 min at 3200×g to 250–500 μL volume, prior to addition of protease-phosphatase inhibitor and 5× sample loading buffer containing 10% DTT. Western blot analysis was adapted from a previous protocol [117]. Briefly, 10–50 μg protein was separated by SDS-PAGE and transferred to PVDF membrane. Membranes were blocked for 1 h with OneBlock Western-CL Blocking Buffer (Genesee, 20–313), and incubated with primary antibodies diluted in OneBlock (Suppl. Table S8) at 4 °C overnight. Membranes were washed 3X in PBST (PBS + 0.1% Tween-20) before adding HRP-conjugated secondary antibodies (Suppl. Table S9) in OneBlock and incubating for 1 h at RT. After 3X wash in PBST, Immobilon Forte substrate (Millipore, #WBLUF0100) was added for 1 min. The membranes were then imaged using the ChemiDoc XRS with Chemi High Resolution setting. Restore Western Blot Stripping Buffer (ThermoFisher, #21059) was used for reprobing.

Cell fractionation

The cell fractionation protocol was adapted from the OptiPrep Application Sheet (S24). Briefly, HUVEC were grown to confluency, rinsed 2X in PBS, 1X in homogenization media (0.25 M sucrose, 1mM EDTA, 10mM HEPES, pH 7.4), and scraped off into homogenization media + 1x protease-phosphatase inhibitor cocktail (Cell Signaling, 5872 S). Cells were passed through a 27-gauge needle 15X to remove nuclei, then the homogenate was centrifuged at 1500×g for 10 min at 4 °C. The cleared supernatant was

added directly to a 2.5–30% iodixanol (OptiPrep, Millipore #D1556) gradient. Solutions of 2.5, 5, 7.5, 10. 12.5, 15, 17.5, 20, or 30% (w/v) iodixanol were prepared with appropriate volumes of homogenization media and 50% iodixanol working solution. The step gradient was formed by bottom loading 13 mL UltraClear tubes (Beckman Coulter, #344059) with a long metal cannula with 800 μL 2.5%, 1.6 mL 5%, 1.6 mL 7.5%, 1.6 mL 10%, 400 μL 12.5%, 1.6 mL 15%, 400 μL 17.5%, 400 μL 20%, and 400 μL 30% iodixanol. The gradients were loaded into a prechilled Beckman SW 41Ti swinging-bucket rotor, then centrifuged at 200,000×g (40,291 rpm) for 2.5 h; decelerated from 2000 rpm without the brake in a Beckman Coulter ultracentrifuge. 400 μL fractions were carefully collected from the tubes by upward displacement and 5X sample loading buffer containing 10% DTT was added to all samples before boiling for 5 min. Samples were stored at −20 °C.

Immunofluorescence staining

Falcon 4-well culture slides (Fisher, #354104) or Ibidi 8-well culture slides (Ibidi, #80807) were coated with 5 μg/mL fibronectin for 45 min at RT before seeding $1.5–3.0×10^5$ cells/well and allowing overnight recovery. Following treatments, cells were rinsed with PBS, fixed in 4% PFA for 10 min, then rinsed with PBS and permeabilized with 0.1% TritonX-100 for 10 min at RT. Cells were rinsed with PBS then blocked for 1 h at RT in blocking solution (5% NBCS + antibiotics + 0.01% Sodium Azide in PBS). Primary antibodies were diluted in blocking solution (Suppl. Table S8) and incubation was at 4 °C for 48 h. Cells were washed with PBS 3X before adding Alexa-Fluor-conjugated secondary antibodies (Suppl. Table S9), DAPI, and Alexa-Fluor-conjugated phalloidin in blocking solution and incubating for 3 h at RT in the dark. Cells were washed with PBS 3X, chambers were removed if applicable, and coverslips were mounted using Prolong Diamond Antifade mounting media and sealed.

Image acquisition

Unless otherwise stated, confocal images were acquired with an Olympus confocal laser scanning microscope and camera (Fluoview FV3000, IX83) and a UPlanSApo 60x oil-immersion objective (NA 1.40) with 1024×1024 resolution and 2x optical zoom. Images were acquired with the Olympus Fluoview FV31S-SW software and all image analysis, including Z-stack compression, was performed in ImageJ or Imaris [118, 119]. Any adjustments to brightness and contrast were performed evenly for all images in an experiment.

High-resolution imaging was performed using a Zeiss 880 confocal with Airyscan FAST and a Plan-Apo 63x oil-immersion objective (NA 1.40). Images were acquired with

the ZEN software and all image analysis was performed in ImageJ or Imaris.

For live cell imaging, tagged sFLT1 (sFLT1-SBP-EGFP) expressing HUVEC seeded in fibronectin-coated glass bottom slides (Ibidi, #80807) were placed in an environmental chamber on an Olympus Fluoview FV3000 and Z-stacks were imaged using FreeRun time-lapse on the UPlanSApo 60x oil-immersion objective (NA 1.40) with 2x optical zoom after the addition of 50 μM D-Biotin (Sigma, B4501). Temporal projections of live-cell imaging were performed using the Temporal-Color Code tool in ImageJ.

3D angiogenesis sprouting model

The 3D sprouting angiogenesis assay was performed as previously described [70, 92]. Briefly, control HUVEC or HUVEC 48 h post-siRNA treatment were incubated with cytodex 3 microcarrier beads (#17048501, GE Healthcare Life Sciences) overnight then resuspended in 2.2 mg/mL fibrinogen (#820224, Fisher) plus aprotinin (A3428, Sigma) and embedded in a fibrin matrix by combining 7 μl of 50U/ml thrombin (T7201-500UN, Sigma) with 500 μl of bead/fibrinogen solution in a 24-well glass-bottomed plate (#662892, Grenier Bio) that was incubated for 30 min at RT then 30 min at 37 °C. EGM-2 and normal human lung fibroblasts (NHLF, CC2512, Lonza) at a concentration of $2×10^5$ cells/mL was added to each well, and incubation was at 37 °C. On day 7 following 18 h of inhibitor treatment or day 4 following siRNA treatment, fibroblasts were removed via trypsin treatment (5X-trypsin for 7 min at 37 °C), and samples were fixed in 4% PFA for 15 min at RT. Samples were permeabilized with 0.5% Triton X-100 in PBS for 1 h at RT. After rinsing in PBS, samples were blocked in: 5% FBS, 1% donkey serum, 1% BSA (A4503, Sigma), 0.3% Triton X-100 (T8787, Sigma) in PBS overnight at 4 °C. Samples were rinsed 3X in PBS, then anti-FLT1 (1:500, RnD) and anti-γ-Adaptin (1:500, abcam) antibodies in antibody solution (5% FBS, 1% BSA, 0.1% Triton X-100) were added for 48 h at 4 °C. Samples were rinsed 3×10 min in 0.5% Tween-20 in PBS then washed overnight at 4 °C in 0.5% Tween-20. Samples were rinsed 3X in PBS, then donkey anti-goat AlexaFluor488 (1:1000, ThermoFisher), donkey anti-rabbit AlexaFluor594 (1:1000, ThermoFisher), DAPI (0.3μM, #10236276001, Sigma) and AlexaFluor647 Phalloidin (1:500, Life Technologies) in blocking solution were added to the wells, and incubation was overnight at 4 °C prior to rinsing 6X in 0.5% Tween in PBS.

For FLT1 localization, images were acquired in the Z-plane using a UPlanSApo 60x oil-immersion objective (NA 1.40). For whole bead analysis, images were acquired in the Z-plane using a UPlanSApo 20x oil-immersion objective (NA 0.58) and processed in ImageJ. The phalloidin channel was used to create a temporal color code relative

to the Z-distance to distinguish overlapping sprouts. The number of sprouts per bead was calculated using the multipoint analysis ImageJ tool. Total vessel area was measured by tracing each vessel from the edge of the bead to the tip of the sprout. The tracing was selected and converted to a mask and skeletonized. The sum of all the vessels measured was calculated using the AnalyzeSkeleton plugin, and the pixels were converted to μm.

Zebrafish

Zebrafish (*Danio rerio*) were housed in an institutional animal care and use committee (IACUC)-approved facility and maintained as previously described [120]. *Tg(fli1a:lifeactEGFP)^mu240* was received through ZFIN [121]. The *TgTm(flt1_E3_HAHA)^ka611* line and the *flt1^enh*:*sflt1_Δ7-HAHA* Tol2 expression construct were generated as described [94]. As previously described [94, 122], 25 ng/uL^{-1}*flt1^enh*:*sflt1_Δ7-HAHA* and 25 ng/uL^{-1} Tol2 transposase mRNA were injected into one-cell stage *Tg(fli1a:lifeactEGFP)^mu240* embryos to generate mosaic expression of tagged sflt1. Tol2 transposase mRNA was generated using the sp6 mMessage mMachine synthesis kit (AM1340, Thermo Fisher). At 26 hpf, *TgTm(flt1_E3_HAHA)^ka611* or *Tg(flt1^enh*:*sflt1_Δ7-HAHA)* embryos were sorted for lifeactEGFP + vasculature, dechorinated, and incubated in E3 buffer containing 100 μM Chlorpromazine or H2O vehicle control for 6 h at 28.5 °C. After treatments, embryos were fixed in ice cold 4% PFA for 2 h at RT or overnight at 4 °C, rinsed 3X with PBS, then permeabilized with 1% Triton-X in PBS for 1 h at RT shaking. Embryos were blocked in 1% Triton-X + 1% BSA + 5% donkey serum in PBS for 2 h at RT shaking. HA antibody (Suppl. Table S8) was diluted in antibody solution (0.5% Triton-X + 1% BSA in PBS) and incubation was 48 h at 4 °C shaking. Embryos were washed with 0.5% Triton-X 4 × 10 min each at RT followed by overnight wash at 4 °C. Secondary antibody and DAPI (Suppl. Table S9) was diluted in antibody solution and incubated for overnight at 4 °C in the dark. Embryos were washed 5X with 0.5% Triton-X for 30 min at RT, rinsed and stored in PBS, then placed onto glass slides for mounting. Heads were removed below the yolk sac with a razor and trunks were mounted in Prolong Diamond Antifade. The slides were cured overnight at RT in the dark before sealing with nail polish.

To mark endothelial cell nuclei, images were imported into Imaris and each Z-plane of the fli1a:lifeactEGFP channel was manually traced to create a new surface. The mask channel tool was then used to mask the DAPI channel within the fli1a:lifeactEGFP surface to visualize the endothelial cell nuclei.

Mechanistic computational model of sFLT1 secretion

To quantitatively characterize sFLT1 secretion kinetics, we built a mechanistic model based on two delay differential equations tracking intracellular sFLT1 protein levels (S_i) and extracellular sFLT1 protein levels (S_x). The model includes four processes—sFLT1 production, secretion, intracellular degradation, and extracellular degradation (Fig. 1G; Suppl. Tables S1–S4). We parameterized the model using two independent previously published sFLT1 secretion time course data sets from experiments using HUVEC: a pulse-chase experiment tracking fold change in both intracellular and extracellular sFLT1 [69]; and an experiment measuring absolute sFLT1 concentration in conditioned media [123]. The resulting parameters (Suppl. Table S3) are also a good fit for the measurements of secreted sFLT1 over time in our study (Fig. 1F). Inhibitor perturbation was simulated by reducing individual parameter values to identify the fractional inhibition of transport processes required to reproduce experimentally observed changes in extracellular sFLT1.

Data quantification

Western blot band relative intensity was determined using densitometry analysis [124]. Images were acquired within the linear range using the ChemiDoc XRS with Chemi High Resolution setting. The images were exported as TIFFs and analyzed using the ImageJ Gels tool. An ROI was created around the first lane and copied to each additional lane of the gel. The intensity profiles of each lane was plotted, and a line was drawn to subtract background signal. The pixel intensity of each lane was measured and compared relative to the control lane. Tubulin or GAPDH was used for loading control normalization.

To analyze Golgi colocalization, a parallel line to the longest Golgi axis was drawn in ImageJ. Single plane intensity data of each channel was fitted to a Gaussian distribution to locate the peak of each channel and was then plotted as a function of distance [125]. For localization near the cell surface or within clathrin-coated vesicles, single plane images were used to generate line scan intensity profiles in ImageJ.

To determine the clathrin intensity within the sFLT1-HA region, single plane images were analyzed in ImageJ. The sFLT1-HA channel was fitted to a Gaussian distribution to obtain the peak intensity region and then a threshold was set to create a mask. The mask was applied to the clathrin channel and average intensity measurements for clathrin within the sFLT1-HA area were acquired. Each sFLT1-HA positive cell per condition across 3 independent experiments was graphed using Prism9 software.

Vesicle analysis in HUVEC with tagged sFLT1 (sFLT1-SBP-EGFP) utilized ROI drawn around labeled cells for area measurement in ImageJ. The EGFP channel was thresholded

and the Analyze Particles function used to count discrete signal within 0.05–20 μm range, then dividing by cell area. Cells from 4 experimental replicates were graphed using Prism9 software.

Statistics

Student's two-tailed *t* test was used to determine the statistical significance in experiments with two groups. One-way ANOVA with Tukey's multiple comparisons test was used to determine statistical significance for experiments with 3 or more groups. Error bars represent the mean $\pm$ standard deviation of $n \geq 3$ independent experiments. Statistical tests and graphs were made using the Prism9 software (GraphPad Software) and R Statistical Software (v 4.0.5, R Core Team, 2021) with the tidyverse package [126].

Declarations

References

1. Carmeliet P (2005) Angiogenesis in life, disease and medicine. Nature 438(7070):932–936. https://doi.org/10.1038/nature04478
2. Potente M, Gerhardt H, Carmeliet P (2011) Basic and therapeutic aspects of angiogenesis. Cell 146(6):873–887. https://doi.org/10.1016/j.cell.2011.08.039
3. Bautch VL, Mukouyama YS (2022) The beauty and complexity of blood vessel patterning. Cold Spring Harb Perspect Med. https://doi.org/10.1101/cshperspect.a041167
4. Adams RH, Alitalo K (2007) Molecular regulation of angiogenesis and lymphangiogenesis. Nat Reviews Mol Cell Biol 8(6):464–478. https://doi.org/10.1038/nrm2183
5. Swift MR, Weinstein BM (2009) Arterial–venous specification during development. Circ Res 104(5):576–588. https://doi.org/10.1161/circresaha.108.188805
6. Bautch VL, Caron KM (2015) Blood and lymphatic vessel formation. Cold Spring Harb Perspect Biol 7(3):a008268. https://doi.org/10.1101/cshperspect.a008268
7. Ferrara N (2005) The role of VEGF in the regulation of physiological and pathological angiogenesis. Birkhäuser Basel. https://doi.org/10.1007/3-7643-7311-3_15
8. Eichmann A, Simons M (2012) VEGF signaling inside vascular endothelial cells and beyond. Curr Opin Cell Biol 24(2):188–193. https://doi.org/10.1016/j.ceb.2012.02.002
9. Bautch VL (2012) VEGF-directed blood vessel patterning: from cells to organism. Cold Spring Harb Perspect Med 2(9):a006452. https://doi.org/10.1101/cshperspect.a006452
10. Shibuya M (2011) Vascular endothelial growth factor (VEGF) and its receptor (VEGFR) signaling in angiogenesis: a crucial target for Anti- and pro-angiogenic therapies. Genes Cancer 2(12):1097–1105. https://doi.org/10.1177/1947601911423031
11. Gerhardt H, Golding M, Fruttiger M, Ruhrberg C, Lundkvist A, Abramsson A, Jeltsch M, Mitchell C, Alitalo K, Shima D, Betsholtz C (2003) VEGF guides angiogenic sprouting utilizing endothelial tip cell filopodia. J Cell Biol 161(6):1163–1177. https://doi.org/10.1083/jcb.200302047
12. Blanco R, Gerhardt H (2013) VEGF and notch in tip and stalk cell selection. Cold Spring Harb Perspect Med 3(1):a006569–a006569. https://doi.org/10.1101/cshperspect.a006569
13. Roca C, Adams RH (2007) Regulation of vascular morphogenesis by notch signaling. Genes Dev 21(20):2511–2524. https://doi.org/10.1101/gad.1589207
14. Kendall RL, Thomas KA (1993) Inhibition of vascular endothelial cell growth factor activity by an endogenously encoded soluble receptor. Proc Natl Acad Sci USA 90(22):10705–10709. https://doi.org/10.1073/pnas.90.22.10705
15. Shibuya M (2001) Structure and dual function of vascular endothelial growth factor receptor-1 (Flt-1). Int J Biochem Cell Biol 33(4):409–420. https://doi.org/10.1016/s1357-2725(01)00026-7
16. Shibuya M (2006) Vascular endothelial growth factor receptor-1 (VEGFR-1/Flt-1): a dual regulator for angiogenesis. Angiogenesis 9(4):225–230. https://doi.org/10.1007/s10456-006-9055-8

17. Simons M, Gordon E, Claesson-Welsh L (2016) Mechanisms and regulation of endothelial VEGF receptor signalling. Nat Rev Mol Cell Biol 17(10):611–625. https://doi.org/10.1038/nrm.2016.87

18. Fong G-H, Rossant J, Gertsenstein M, Breitman ML (1995) Role of the Flt-1 receptor tyrosine kinase in regulating the assembly of vascular endothelium. Nature 376(6535):66–70. https://doi.org/10.1038/376066a0

19. Carmeliet P, Ferreira V, Breier G, Pollefeyt S, Kieckens L, Gertsenstein M, Fahrig M, Vandenhoeck A, Harpal K, Eberhardt C, Declercq C, Pawling J, Moons L, Collen D, Risau W, Nagy A (1996) Abnormal blood vessel development and lethality in embryos lacking a single VEGF allele. Nature 380(6573):435–439. https://doi.org/10.1038/380435a0

20. Ferrara N, Carver-Moore K, Chen H, Dowd M, Lu L, O'Shea KS, Powell-Braxton L, Hillan KJ, Moore MW (1996) Heterozygous embryonic lethality induced by targeted inactivation of the VEGF gene. Nature 380(6573):439–442. https://doi.org/10.1038/380439a0

21. Shalaby F, Rossant J, Yamaguchi TP, Gertsenstein M, Wu X-F, Breitman ML, Schuh AC (1995) Failure of blood-island formation and vasculogenesis in Flk-1-deficient mice. Nature 376(6535):62–66. https://doi.org/10.1038/376062a0

22. Hiratsuka S, Minowa O, Kuno J, Noda T, Shibuya M (1998) Flt-1 lacking the tyrosine kinase domain is sufficient for normal development and angiogenesis in mice. Proc Natl Acad Sci USA 95(16):9349–9354. https://doi.org/10.1073/pnas.95.16.9349

23. Hiratsuka S, Nakao K, Nakamura K, Katsuki M, Maru Y, Shibuya M (2005) Membrane fixation of vascular endothelial growth factor receptor 1 ligand-binding domain is important for vasculogenesis and angiogenesis in mice. Mol Cell Biol 25(1):346–354. https://doi.org/10.1128/MCB.25.1.346-354.2005

24. Grunewald M, Kumar S, Sharife H, Volinsky E, Gileles-Hillel A, Licht T, Permyakova A, Hinden L, Azar S, Friedmann Y, Kupetz P, Tzuberi R, Anisimov A, Alitalo K, Horwitz M, Leebhoff S, Khoma OZ, Hlushchuk R, Djonov V, Abramovitch R, Tam J, Keshet E (2021) Counteracting age-related VEGF signaling insufficiency promotes healthy aging and extends life span. Science. https://doi.org/10.1126/science.abc8479

25. Di Marco GS, Reuter S, Hillebrand U, Amler S, König M, Larger E, Oberleithner H, Brand E, Pavenstädt H, Brand M (2009) The soluble VEGF receptor sFlt1 contributes to endothelial dysfunction in CKD. J Am Soc Nephrol 20(10):2235–2245. https://doi.org/10.1681/asn.2009010061

26. Giardini V, Carrer A, Casati M, Contro E, Vergani P, Gambacorti-Passerini C (2020) Increased sFLT-1 / PlGF ratio in COVID-19: a novel link to angiotensin II -mediated endothelial dysfunction. Am J Hematol. https://doi.org/10.1002/ajh.25882

27. Dupont V, Kanagaratnam L, Goury A, Poitevin G, Bard M, Julien G, Bonnivard M, Champenois V, Noel V, Mourvillier B, Nguyen P (2021) Excess Soluble fms-like tyrosine kinase 1 correlates with endothelial dysfunction and organ failure in critically ill coronavirus disease 2019 patients. Clin Infect Dis 72(10):1834–1837. https://doi.org/10.1093/cid/ciaa1007

28. Park M, Lee ST (1999) The fourth immunoglobulin-like loop in the extracellular domain of FLT-1, a VEGF receptor, includes a major heparin-binding site. Biochem Biophys Res Commun 264(3):730–734. https://doi.org/10.1006/bbrc.1999.1580

29. Eilken HM, Diéguez-Hurtado R, Schmidt I, Nakayama M, Jeong H-W, Arf H, Adams S, Ferrara N, Adams RH (2017) Pericytes regulate VEGF-induced endothelial sprouting through VEGFR1. Nat Commun. https://doi.org/10.1038/s41467-017-01738-3

30. Barleon B, Reusch P, Totzke F, Herzog C, Keck C, Martiny-Baron G, Marmé D (2001) Soluble VEGFR-1 secreted by endothelial cells and monocytes is present in human serum and plasma from healthy donors. Angiogenesis 4(2):143–154. https://doi.org/10.1023/a:1012245307884

31. Jin J, Sison K, Li C, Tian R, Wnuk M, Sung HK, Jeansson M, Zhang C, Tucholska M, Jones N, Kerjaschki D, Shibuya M, Fantus IG, Nagy A, Gerber HP, Ferrara N, Pawson T, Quaggin SE (2012) Soluble FLT1 binds lipid microdomains in podocytes to control cell morphology and glomerular barrier function. Cell 151(2):384–399. https://doi.org/10.1016/j.cell.2012.08.037

32. Dumont DJ, Fong G-H, Puri MC, Gradwohl G, Alitalo K, Breitman ML (1995) Vascularization of the mouse embryo: a study of flk-1, tek, tie, and vascular endothelial growth factor expression during development. Dev Dyn 203(1):80–92. https://doi.org/10.1002/aja.1002030109

33. Clark DE, Smith SK, Sharkey AM, Charnock-Jones DS (1996) Localization of VEGF and expression of its receptors flt and KDR in human placenta throughout pregnancy. Hum Reprod 11(5):1090–1098. https://doi.org/10.1093/oxfordjournals.humrep.a019303

34. Barleon B, Sozzani S, Zhou D, Weich HA, Mantovani A, Marmé D (1996) Migration of human monocytes in response to vascular endothelial growth factor (VEGF) is mediated via the VEGF receptor flt-1. Blood 87(8):3336–3343

35. Sato W, Kosugi T, Zhang L, Roncal CA, Heinig M, Campbell-Thompson M, Yuzawa Y, Atkinson MA, Grant MB, Croker BP, Nakagawa T (2008) The pivotal role of VEGF on glomerular macrophage infiltration in advanced diabetic nephropathy. Lab Invest 88(9):949–961. https://doi.org/10.1038/labinvest.2008.60

36. Kappas NC, Zeng G, Chappell JC, Kearney JB, Hazarika S, Kallianos KG, Patterson C, Annex BH, Bautch VL (2008) The VEGF receptor Flt-1 spatially modulates Flk-1 signaling and blood vessel branching. J Cell Biol 181(5):847–858. https://doi.org/10.1083/jcb.200709114

37. Chappell JC, Taylor SM, Ferrara N, Bautch VL (2009) Local guidance of emerging vessel sprouts requires soluble Flt-1. Dev Cell 17(3):377–386. https://doi.org/10.1016/j.devcel.2009.07.011

38. Chappell JC, Darden J, Payne LB, Fink K, Bautch VL (2019) Blood vessel patterning on retinal astrocytes requires endothelial Flt-1 (VEGFR-1). J Dev Biol 7(3):18. https://doi.org/10.3390/jdb7030018

39. Matsuoka RL, Marass M, Avdesh A, Helker CS, Maischein HM, Grosse AS, Kaur H, Lawson ND, Herzog W, Stainier DY (2016) Radial glia regulate vascular patterning around the developing spinal cord. eLife. https://doi.org/10.7554/eLife.20253

40. Wild R, Klems A, Takamiya M, Hayashi Y, Strahle U, Ando K, Mochizuki N, van Impel A, Schulte-Merker S, Krueger J, Preau L, le Noble F (2017) Neuronal sFlt1 and vegfaa determine venous sprouting and spinal cord vascularization. Nat Commun 8:13991. https://doi.org/10.1038/ncomms13991

41. Palade G (1975) Intracellular aspects of the process of protein synthesis. Science 189(4200):347–358. https://doi.org/10.1126/science.1096303

42. Bonifacino JS, Glick BS (2004) The mechanisms of vesicle budding and fusion. Cell 116(2):153–166. https://doi.org/10.1016/s0092-8674(03)01079-1

43. Sanderfoot AA, Raikhel NV (1999) The specificity of vesicle trafficking: coat proteins and SNAREs. Plant Cell 11(4):629–641. https://doi.org/10.2307/3870889

44. Nakatsu F, Ohno H (2003) Adaptor protein complexes as the key regulators of protein sorting in the post-Golgi network. Cell Struc Funct 28(5):419–429. https://doi.org/10.1247/csf.28.419

45. Cai H, Reinisch K, Ferro-Novick S (2007) Coats, tethers, rabs, and SNAREs work together to mediate the intracellular destination of a transport vesicle. Dev Cell 12(5):671–682. https://doi.org/10.1016/j.devcel.2007.04.005

46. Nielsen E, Cheung AY, Ueda T (2008) The regulatory RAB and ARF GTPases for vesicular trafficking. Plant Physiol 147(4):1516–1526. https://doi.org/10.1104/pp.108.121798

47. Stenmark H (2009) Rab GTPases as coordinators of vesicle traffic. Nat Rev Mol Cell Biol 10(8):513–525. https://doi.org/10.1038/nrm2728

48. Han J, Pluhackova K, Böckmann RA (2017) The multifaceted role of SNARE proteins in membrane fusion. Front Physiol. https://doi.org/10.3389/fphys.2017.00005

49. Adarska P, Wong-Dilworth L, Bottanelli F (2021) ARF GTPases and their ubiquitous role in intracellular trafficking beyond the golgi. Front Cell Dev Biol 9:679046. https://doi.org/10.3389/fcell.2021.679046

50. Kuliawat R, Arvan P (1992) Protein targeting via the "constitutive-like" secretory pathway in isolated pancreatic islets: passive sorting in the immature granule compartment. J Cell Biol 118(3):521–529. https://doi.org/10.1083/jcb.118.3.521

51. Dittie AS, Hajibagheri N, Tooze SA (1996) The AP-1 adaptor complex binds to immature secretory granules from PC12 cells, and is regulated by ADP-ribosylation factor. J Cell Biol 132(4):523–536. https://doi.org/10.1083/jcb.132.4.523

52. Klumperman J, Kuliawat R, Griffith JM, Geuze HJ, Arvan P (1998) Mannose 6–phosphate receptors are sorted from immature secretory granules via adaptor protein AP-1, clathrin, and syntaxin 6–positive vesicles. J Cell Biol 141(2):359–371. https://doi.org/10.1083/jcb.141.2.359

53. Wendler F, Page L, Urbé S, Tooze SA (2001) Homotypic fusion of immature secretory granules during maturation requires syntaxin 6. Mol Biol Cell 12(6):1699–1709. https://doi.org/10.1091/mbc.12.6.1699

54. Kuliawat R, Kalinina E, Bock J, Fricker L, McGraw TE, Kim SR, Zhong J, Scheller R, Arvan P (2004) Syntaxin-6 SNARE involvement in secretory and endocytic pathways of cultured pancreatic β-Cells. Mol Biol Cell 15(4):1690–1701. https://doi.org/10.1091/mbc.e03-08-0554

55. Lui-Roberts WWY, Collinson LM, Hewlett LJ, Michaux GG, Cutler DF (2005) An AP-1/clathrin coat plays a novel and essential role in forming the Weibel-Palade bodies of endothelial cells. J Cell Biol 170(4):627–636. https://doi.org/10.1083/jcb.200503054

56. Weibel ER, Palade GE (1964) New cytoplasmic components in arterial endothelia. J Cell Biol 23(1):101–112. https://doi.org/10.1083/jcb.23.1.101

57. van Mourik JA, Romani de Wit T, Voorberg J (2002) Biogenesis and exocytosis of Weibel-Palade bodies. Histochem Cell Biol 117(2):113–122. https://doi.org/10.1007/s00418-001-0368-9

58. Lowenstein CJ, Morrell CN, Yamakuchi M (2005) Regulation of Weibel-Palade body exocytosis. Trends Cardiovasc Med 15(8):302–308. https://doi.org/10.1016/j.tcm.2005.09.005

59. Pulido IR, Jahn R, Gerke V (2011) VAMP3 is associated with endothelial weibel-palade bodies and participates in their ca(2+)-dependent exocytosis. Biochim Biophys Acta 1813(5):1038–1044. https://doi.org/10.1016/j.bbamcr.2010.11.007

60. Zhu Q, Yamakuchi M, Lowenstein CJ (2015) SNAP23 regulates endothelial exocytosis of von Willebrand factor. PLoS ONE 10(8):e0118737. https://doi.org/10.1371/journal.pone.0118737

61. Giblin JP, Hewlett LJ, Hannah MJ (2008) Basal secretion of von Willebrand factor from human endothelial cells. Blood 112(4):957–964. https://doi.org/10.1182/blood-2007-12-130740

62. Lopes Da Silva M, Cutler DF (2016) von Willebrand factor multimerization and the polarity of secretory pathways in endothelial cells. Blood 128(2):277–285. https://doi.org/10.1182/blood-2015-10-677054

63. Holthenrich A, Drexler HCA, Chehab T, Naß J, Gerke V (2019) Proximity proteomics of endothelial Weibel-Palade bodies identifies novel regulator of von Willebrand factor secretion. Blood 134(12):979–982. https://doi.org/10.1182/blood.2019000786

64. Kendall RL, Wang G, Thomas KA (1996) Identification of a natural soluble form of the vascular endothelial growth factor receptor, FLT-1, and its heterodimerization with KDR. Biochem Biophys Res Commun 226(2):324–328. https://doi.org/10.1006/bbrc.1996.1355

65. Gruemmer R, Motejlek K, Berghaus D, Weich HA, Neulen J (2005) Regulation of soluble vascular endothelial growth factor receptor (sFlt-1/sVEGFR-1) expression and release in endothelial cells by human follicular fluid and granulosa cells. Reprod Biol Endocrinol 3(1):57. https://doi.org/10.1186/1477-7827-3-57

66. Tuder RM, Flook BE, Voelkel NF (1995) Increased gene expression for VEGF and the VEGF receptors KDR/Flk and flt in lungs exposed to acute or to chronic hypoxia. Modulation of gene expression by nitric oxide. J Clin Invest 95(4):1798–1807. https://doi.org/10.1172/jci117858

67. Gerber H-P, Condorelli F, Park J, Ferrara N (1997) Differential transcriptional regulation of the two vascular endothelial growth factor receptor genes. J Biol Chem 272(38):23659–23667. https://doi.org/10.1074/jbc.272.38.23659

68. Nevo O, Soleymanlou N, Wu Y, Xu J, Kingdom J, Many A, Zamudio S, Caniggia I (2006) Increased expression of sFlt-1 in in vivo and in vitro models of human placental hypoxia is mediated by HIF-1. Am J Physiol Regul Integr Compar Physiol 291(4):R1085–R1093. https://doi.org/10.1152/ajpregu.00794.2005

69. Jung J-J, Tiwari A, Inamdar SM, Thomas CP, Goel A, Choudhury A (2012) Secretion of Soluble Vascular endothelial growth factor receptor 1 (sVEGFR1/sFlt1) requires Arf1, Arf6, and Rab11 GTPases. PLoS ONE 7(9):e44572. https://doi.org/10.1371/journal.pone.0044572

70. Nesmith JE, Chappell JC, Cluceru JG, Bautch VL (2017) Blood vessel anastomosis is spatially regulated by Flt1 during angiogenesis. Development 144(5):889–896. https://doi.org/10.1242/dev.145672

71. Hakkert BC, Rentenaar JM, van Mourik JA (1992) Monocytes enhance endothelial von Willebrand factor release and prostacyclin production with different kinetics and dependency on intercellular contact between these two cell types. Br J Haematol 80(4):495–503. https://doi.org/10.1111/j.1365-2141.1992.tb04563.x

72. O'Mahony L, Holland J, Jackson J, Feighery C, Hennessy TP, Mealy K (1998) Quantitative intracellular cytokine measurement: age-related changes in proinflammatory cytokine production. Clin Exp Immunol 113(2):213–219. https://doi.org/10.1046/j.1365-2249.1998.00641.x

73. Rehman J, Traktuev D, Li J, Merfeld-Clauss S, Temm-Grove CJ, Bovenkerk JE, Pell CL, Johnstone BH, Considine RV, March KL (2004) Secretion of angiogenic and antiapoptotic factors by human adipose stromal cells. Circulation 109(10):1292–1298. https://doi.org/10.1161/01.Cir.0000121425.42966.F1

74. Salmon SE, Smith BA (1970) Immunoglobulin synthesis and total body tumor cell number in IgG multiple myeloma. J Clin Invest 49(6):1114–1121. https://doi.org/10.1172/jci106327

75. Chen LL, Redman CM (1977) Synthesis and secretion of albumin by a synchronized rat hepatoma cell line. Biochim Biophys Acta 479(1):53–68. https://doi.org/10.1016/0005-2787(77)90125-3

76. Janossy G, de la Gomez E, Luquetti A, Snajdr MJ, Waxdal MJ, Platts-Mills TA (1977) T-cell regulation of immunoglobulin synthesis and proliferation in pokeweed (Pa-1)-stimulated human lymphocyte cultures. Scand J Immunol 6(1–2):109–123. https://doi.org/10.1111/j.1365-3083.1977.tb00326.x

77. Werner-Favre C, Matthes T, Barnet M, Zubler RH (1993) High IgE secretion capacity of human plasma cells. Eur J Immunol 23(8):2038–2040. https://doi.org/10.1002/eji.1830230849

78. Bromage ES, Ye J, Owens L, Kaattari IM, Kaattari SL (2004) Use of staphylococcal protein A in the analysis of teleost immunoglobulin structural diversity. Dev Comp Immunol 28(7–8):803–814. https://doi.org/10.1016/j.dci.2003.12.001

79. Bromage E, Stephens R, Hassoun L (2009) The third dimension of ELISPOTs: quantifying antibody secretion from individual plasma cells. J Immunol Method 346(1–2):75–79. https://doi.org/10.1016/j.jim.2009.05.005

80. Mittar S, Ulyatt C, Howell GJ, Bruns AF, Zachary I, Walker JH, Ponnambalam S (2009) VEGFR1 receptor tyrosine kinase localization to the golgi apparatus is calcium-dependent. Exp Cell Res 315(5):877–889. https://doi.org/10.1016/j.yexcr.2008.12.020

81. Mettlen M, Chen P-H, Srinivasan S, Danuser G, Schmid SL (2018) Regulation of clathrin-mediated endocytosis. Annu Rev Biochem 87(1):871–896. https://doi.org/10.1146/annurev-biochem-062917-012644

82. Gurunathan S (2002) Dynamin and clathrin are required for the biogenesis of a distinct class of secretory vesicles in yeast. EMBO J 21(4):602–614. https://doi.org/10.1093/emboj/21.4.602

83. Ponnambalam S, Baldwin SA (2003) Constitutive protein secretion from the trans -golgi network to the plasma membrane (review). Mol Membr Biol 20(2):129–139. https://doi.org/10.1080/0968768031000084172

84. González-Jamett A, Momboisse F, Haro-Acuña V, Bevilacqua J, Caviedes P, Cárdenas A (2013) Dynamin-2 function and dysfunction along the secretory pathway. Front Endocrinol. https://doi.org/10.3389/fendo.2013.00126

85. Park SY, Guo X (2014) Adaptor protein complexes and intracellular transport. Biosci Rep. https://doi.org/10.1042/bsr20140069

86. Kockx M, Karunakaran D, Traini M, Xue J, Huang KY, Nawara D, Gaus K, Jessup W, Robinson PJ, Kritharides L (2014) Pharmacological inhibition of dynamin II reduces constitutive protein secretion from primary human macrophages. PLoS ONE 9(10):e111186. https://doi.org/10.1371/journal.pone.0111186

87. Morrell CN, Matsushita K, Lowenstein CJ (2005) A novel inhibitor of N-ethylmaleimide-sensitive factor decreases leukocyte trafficking and peritonitis. J Pharmacol Exp Ther 314(1):155–161. https://doi.org/10.1124/jpet.104.082529

88. Alonso MA, MilláN J (2001) The role of lipid rafts in signalling and membrane trafficking in *T. lymphocytes*. J Cell Sci 114(22):3957–3965. https://doi.org/10.1242/jcs.114.22.3957

89. Lingwood D, Simons K (2010) Lipid rafts as a membrane-organizing principle. Science 327(5961):46–50. https://doi.org/10.1126/science.1174621

90. Sporn LA, Marder VJ, Wagner DD (1986) Inducible secretion of large, biologically potent von willebrand factor multimers. Cell 46(2):185–190. https://doi.org/10.1016/0092-8674(86)90735-x

91. Tsai H-M, Nagel RL, Hatcher VB, Seaton AC, Sussman II (1991) The high molecular weight form of endothelial cell von willebrand factor is released by the regulated pathway. Br J Haematol 79(2):239–245. https://doi.org/10.1111/j.1365-2141.1991.tb04528.x

92. Nakatsu MN, Hughes CC (2008) An optimized three-dimensional in vitro model for the analysis of angiogenesis. Methods Enzymol 443:65–82. https://doi.org/10.1016/s0076-6879(08)02004-1

93. Buglak DB, Kushner EJ, Marvin AP, Davis KL, Bautch VL (2020) Excess centrosomes disrupt vascular lumenization and endothelial cell adherens junctions. Angiogenesis 23(4):567–575. https://doi.org/10.1007/s10456-020-09737-7

94. Klems A, Van Rijssel J, Ramms AS, Wild R, Hammer J, Merkel M, Derenbach L, Préau L, Hinkel R, Suarez-Martinez I, Schulte-Merker S, Vidal R, Sauer S, Kivelä R, Alitalo K, Kupatt C, Van Buul JD, Le Noble F (2020) The GEF Trio controls endothelial cell size and arterial remodeling downstream of Vegf signaling in both zebrafish and cell models. Nat Commun. https://doi.org/10.1038/s41467-020-19008-0

95. Burgess TL, Kelly RB (1987) Constitutive and regulated secretion of proteins. Ann Rev Cell Biol 3(1):243–293. https://doi.org/10.1146/annurev.cb.03.110187.001331

96. Ang AL, Taguchi T, Francis S, Fölsch H, Murrells LJ, Pypaert M, Warren G, Mellman I (2004) Recycling endosomes can serve as intermediates during transport from the golgi to the plasma membrane of MDCK cells. J Cell Biol 167(3):531–543. https://doi.org/10.1083/jcb.200408165

97. Jopling H, Odell A, Pellet-Many C, Latham A, Frankel P, Sivaprasadarao A, Walker J, Zachary I, Ponnambalam S (2014) Endosome-to-plasma membrane recycling of VEGFR2 receptor tyrosine kinase regulates endothelial function and blood vessel formation. Cells 3(2):363–385. https://doi.org/10.3390/cells3020363

98. Naß J, Terglane J, Gerke V (2021) Weibel Palade bodies: unique secretory organelles of endothelial cells that control blood vessel homeostasis. Front Cell Dev Biol. https://doi.org/10.3389/fcell.2021.813995

99. Raghavan S, Brishti MA, Leo MD (2022) Rab GTPases as modulators of vascular function. Cells 11(19):3061. https://doi.org/10.3390/cells11193061

100. Nightingale TD, Pattni K, Hume AN, Seabra MC, Cutler DF (2009) Rab27a and MyRIP regulate the amount and multimeric state of VWF released from endothelial cells. Blood 113(20):5010–5018. https://doi.org/10.1182/blood-2008-09-181206

101. Bierings R, Hellen N, Kiskin N, Knipe L, Fonseca A-V, Patel B, Meli A, Rose M, Hannah MJ, Carter T (2012) The interplay between the Rab27A effectors Slp4-a and MyRIP controls hormone-evoked Weibel-Palade body exocytosis. Blood 120(13):2757–2767. https://doi.org/10.1182/blood-2012-05-429936

102. Bock JB, Klumperman J, Davanger S, Scheller RH (1997) Syntaxin 6 functions in trans-golgi network vesicle trafficking. Mol Biol Cell 8(7):1261–1271. https://doi.org/10.1091/mbc.8.7.1261

103. Manickam V, Tiwari A, Jung JJ, Bhattacharya R, Goel A, Mukhopadhyay D, Choudhury A (2011) Regulation of vascular endothelial growth factor receptor 2 trafficking and angiogenesis by golgi localized t-SNARE syntaxin 6. Blood 117(4):1425–1435. https://doi.org/10.1182/blood-2010-06-291690

104. Schillemans M, Karampini E, Van Den Eshof BL, Gangaev A, Hofman M, Van Breevoort D, Meems H, Janssen H, Mulder AA, Jost CR, Escher JC, Adam R, Carter T, Koster AJ, Van Den Biggelaar M, Voorberg J, Bierings R (2018) Weibel-Palade body localized Syntaxin-3 modulates Von Willebrand factor secretion from endothelial cells. Arterioscler Thromb Vasc Biol 38(7):1549–1561. https://doi.org/10.1161/atvbaha.117.310701

105. Schillemans M, Karampini E, Kat M, Bierings R (2019) Exocytosis of Weibel–Palade bodies: how to unpack a vascular emergency kit. J Thromb Haemost 17(1):6–18. https://doi.org/10.1111/jth.14322

106. Chappell JC, Cluceru JG, Nesmith JE, Mouillesseaux KP, Bradley VB, Hartland CM, Hashambhoy-Ramsay YL, Walpole J, Peirce SM, Mac Gabhann F, Bautch VL (2016) Flt-1 (VEGFR-1) coordinates discrete stages of blood vessel formation. Cardiovasc Res 111(1):84–93. https://doi.org/10.1093/cvr/cvw091

107. Boucher JM, Clark RP, Chong DC, Citrin KM, Wylie LA, Bautch VL (2017) Dynamic alterations in decoy VEGF receptor-1 stability regulate angiogenesis. Nat Commun 8:15699. https://doi.org/10.1038/ncomms15699

108. Riggs KA, Hasan N, Humphrey D, Raleigh C, Nevitt C, Corbin D, Hu C (2012) Regulation of integrin endocytic recycling and Chemotactic Cell Migration by Syntaxin 6 and VAMP3 Interaction. J Cell Sci 125(16):3827–3839. https://doi.org/10.1242/jcs.102566

109. D'Souza-Schorey C, Chavrier P (2006) ARF proteins: roles in membrane traffic and beyond. Nat Rev Mol Cell Biol 7(5):347–358. https://doi.org/10.1038/nrm1910

110. Boncompain G, Divoux S, Gareil N, De Forges H, Lescure A, Latreche L, Mercanti V, Jollivet F, Raposo G, Perez F (2012) Synchronization of secretory protein traffic in populations of cells. Nat Methods 9(5):493–498. https://doi.org/10.1038/nmeth.1928

111. Fourriere L, Kasri A, Gareil N, Bardin S, Bousquet H, Pereira D, Perez F, Goud B, Boncompain G, Miserey-Lenkei S (2019) RAB6 and microtubules restrict protein secretion to focal adhesions. J Cell Biol 218(7):2215–2231. https://doi.org/10.1083/jcb.201805002

112. Pereira C, Stalder D, Anderson GSF, Shun-Shion AS, Houghton J, Antrobus R, Chapman MA, Fazakerley DJ, Gershlick DC (2023) The exocyst complex is an essential component of the mammalian constitutive secretory pathway. J Cell Biol. https://doi.org/10.1083/jcb.202205137

113. Wu FTH, Stefanini MO, Mac Gabhann F, Popel AS (2009) A compartment model of VEGF distribution in humans in the presence of soluble VEGF receptor-1 acting as a ligand trap. PLoS ONE 4(4):e5108. https://doi.org/10.1371/journal.pone.0005108

114. Kuliawat R, Arvan P (1994) Distinct molecular mechanisms for protein sorting within immature secretory granules of pancreatic beta-cells. J Cell Biol 126(1):77–86. https://doi.org/10.1083/jcb.126.1.77

115. Metcalf DJ, Nightingale TD, Zenner HL, Lui-Roberts WW, Cutler DF (2008) Formation and function of Weibel-Palade bodies. J Cell Sci 121(1):19–27. https://doi.org/10.1242/jcs.03494

116. Raja E, Tzavlaki K, Vuilleumier R, Edlund K, Kahata K, Zieba A, Morén A, Watanabe Y, Voytyuk I, Botling J, Söderberg O, Micke P, Pyrowolakis G, Heldin CH, Moustakas A (2016) The protein kinase LKB1 negatively regulates bone morphogenetic protein receptor signaling. Oncotarget 7(2):1120–1143. https://doi.org/10.18632/oncotarget.6683

117. Mahmood T, Yang PC (2012) Western blot: technique, theory, and trouble shooting. N Am J Med Sci 4(9):429–434. https://doi.org/10.4103/1947-2714.100998

118. Linkert M, Rueden CT, Allan C, Burel J-M, Moore W, Patterson A, Loranger B, Moore J, Neves C, Macdonald D, Tarkowska A, Sticco C, Hill E, Rossner M, Eliceiri KW, Swedlow JR (2010) Metadata matters: access to image data in the real world. J Cell Biol 189(5):777–782. https://doi.org/10.1083/jcb.201004104

119. Schindelin J, Arganda-Carreras I, Frise E, Kaynig V, Longair M, Pietzsch T, Preibisch S, Rueden C, Saalfeld S, Schmid B, Tinevez J-Y, White DJ, Hartenstein V, Eliceiri K, Tomancak P, Cardona A (2012) Fiji: an open-source platform for biological-image analysis. Nat Methods 9(7):676–682. https://doi.org/10.1038/nmeth.2019

120. Wiley DM, Kim J-D, Hao J, Hong CC, Bautch VL, Jin S-W (2011) Distinct signalling pathways regulate sprouting angiogenesis from the dorsal aorta and the axial vein. Nat Cell Biol 13(6):686–692. https://doi.org/10.1038/ncb2232

121. Hamm MJ, Kirchmaier BC, Herzog W (2016) Sema3d controls collective endothelial cell migration by distinct mechanisms via Nrp1 and PlxnD1. J Cell Biol 215(3):415–430. https://doi.org/10.1083/jcb.201603100

122. Mouillesseaux KP, Wiley DS, Saunders LM, Wylie LA, Kushner EJ, Chong DC, Citrin KM, Barber AT, Park Y, Kim J-D, Samsa LA, Kim J, Liu J, Jin S-W, Bautch VL (2016) Notch regulates BMP responsiveness and lateral branching in vessel networks via SMAD6. Nat Commun 7(1):13247. https://doi.org/10.1038/ncomms13247

123. Hornig C, Barleon B, Ahmad S, Vuorela P, Ahmed A, Weich HA (2000) Release and complex formation of Soluble VEGFR-1 from endothelial cells and biological fluids. Lab Invest 80(4):443–454. https://doi.org/10.1038/labinvest.3780050

124. Taylor SC, Berkelman T, Yadav G, Hammond M (2013) A defined methodology for reliable quantification of western blot data. Mol Biotech 55(3):217–226. https://doi.org/10.1007/s12033-013-9672-6

125. Hummer BH, Maslar D, Soltero-Gutierrez M, De Leeuw NF, Asensio CS (2020) Differential sorting behavior for soluble and transmembrane cargoes at the trans-golgi network in endocrine cells. Mol Biol Cell 31(3):157–166. https://doi.org/10.1091/mbc.e19-10-0561

126. Wickham H, Averick M, Bryan J, Chang W, McGowan L, François R, Grolemund G, Hayes A, Henry L, Hester J, Kuhn M, Pedersen T, Miller E, Bache S, Müller K, Ooms J, Robinson D, Seidel D, Spinu V, Takahashi K, Vaughan D, Wilke C, Woo K, Yutani H (2019) Welcome to the Tidyverse. J Open Source Software 4(43):1686. https://doi.org/10.21105/joss.01686